1 Stratospheric circulation response to large Northern high-latitude volcanic eruptions in a global

2 climate model

3

4

Hera Guðlaugsdóttir^{1,2}, Yannick Peings², Davide Zanchettin³, Gudrun Magnusdottir²

- ¹University of Iceland, institute of Earth Sciences, 102 Reykjavík, Iceland
- 6 ²University of California Irvine, Department of Earth System Science, Irvine CA 92697-3100,
- 7 United States
- 8 3University Ca'Foscari of Venice, department of Environmental Sciences, Informatics and
- 9 Statistics, 30123 Venice, Italy
- 10 Correspondence to: Hera Guðlaugsdóttir (hera@hi.is)

11 12

13 14

24

25

26

27

28

31

32

33

15 Abstrac

Stratospheric aerosols, after major explosive volcanic eruptions can trigger climate anomalies for up to several years following such events. Whereas the mechanisms responsible for the prolonged response to volcanic surface cooling have been extensively investigated for tropical eruptions, less is known about the dynamical response to high-latitude eruptions. Here we use global climate model simulations of an idealized 6 month long northern hemisphere high-latitude eruption to investigate the stratospheric circulation response during the first three post-eruption winters. Two model configurations are used, coupled with an interactive ocean, and, with prescribed sea surface temperature. Our results reveal significant differences in the response of the polar stratosphere with an interactive ocean; the surface cooling is enhanced and zonal

the response of the polar stratosphere with an interactive ocean: the surface cooling is enhanced and zonal flow anomalies are stronger in the troposphere, which impacts atmospheric waveguides and upward propagation of large-scale planetary waves. We identify two competing mechanisms contributing to the post-eruption evolution of the polar vortex: 1) A local stratospheric top-down mechanism whereby increased absorption of aerosol-induced thermal radiation yields a polar vortex strengthening via thermal wind response; 2) A bottom-up mechanism whereby anomalous surface cooling yields a wave-activity flux

increase that propagates into the winter stratosphere. We detect unusually high frequency of Sudden Stratospheric Warmings in the idealized forcing simulation with interactive ocean that calls for further

exploration. In the coupled runs, the top-down mechanism dominates over the bottom-up mechanism in

winter 1, while the bottom-up mechanism dominates in the follow-up winters.

Deleted:

Deleted: The temporary enhancement of the

Deleted: s

Deleted: layer

Deleted: ,

Deleted: or

Deleted: This causes a weakening of the polar vortex and an increase in the occurrence of sudden stratospheric warming events (SSWs), although with a small signal-to-noise ratio.

1 Introduction

44 45

46

47

48

49

50

51

52

53

54

55

56

57

58

59

60

61

62

63

64

65

66

67

68

69

70

71

72

73

43

The enhancement of the stratospheric aerosol layer following strong sulfur-rich explosive volcanic eruptions, is an important driver of natural climate variability due to the short-lived yet possibly very strong radiative anomalies imposed within the atmospheric column (Robock, 2000; Timmreck, 2012; Zanchettin, 2017). This direct radiative effect can alter both meridional surface and stratospheric temperature gradients that can, in turn, initiate further dynamical climate responses on seasonal to decadal time scales (Church et al., 2005; Gleckler et al., 2006; Stenchikov et al., 2009; Shindell et al., 2009; Otterå et al., 2010; Zanchettin et al., 2012; Swingedouw et al., 2015). Direct radiative and dynamical responses critically depend on the spatiotemporal characteristics of the enhanced stratospheric aerosol layer, which ultimately depends on the characteristics of the eruption, such as magnitude, timing and location (Stenchikov et al., 2009; Shindell et al., 2009; Zanchettin et al., 2012; Swingedouw et al., 2015). Spatiotemporal characteristics of volcanic aerosol from high-latitude (HL), Northern Hemisphere (NH) eruptions are typically very different when compared to tropical eruptions. Accordingly, several studies have shown that HL eruptions typically initiate different climate responses compared to tropical eruptions (Meronen et al., 2012; Pausata et al., 2015; Guðlaugsdóttir et al., 2018; Zambri et al., 2019; Sjolte et al., 2021). Therefore, tropical eruptions cannot be considered close analogs of HL eruptions, underlining the need for more studies on the latter to further quantify their potential climate impacts (Zanchettin et al., 2016). In this study we explore how stratospheric sulfate aerosol enhancements largely constrained in the NH extratropics affect hemispheric-scale atmospheric dynamics, with a focus on the stratospheric polar vortex and on temporal evolution of responses through three perturbed winters.

The winter stratospheric polar vortex is considered to play a deciding role in distinguishing between the response to low- and HL NH enhancements of the stratospheric sulfate aerosol layer, where opposite responses are expected to emerge under the same mechanism: When the stratospheric sulfate aerosol layer is enhanced at low latitudes, e.g., following tropical volcanic eruptions, local warming by infrared absorption increases the meridional stratospheric temperature gradient that can lead to a stratospheric polar vortex strengthening due to a thermal wind response (e.g., Zanchettin et al., 2012; Bittner et al., 2016). Conversely, the local warming from aerosols constrained at higher latitudes decreases the meridional temperature gradient, promoting a

Deleted:

Deleted: , which typically occurs

Deleted:

Deleted: by imposing

Deleted: high-latitude NH

Deleted: high-latitude NH

Deleted: high-latitude

82 weakening of the polar vortex (Kodera, 1994; Perlwitz & Graf, 1995; Stenchikov et al., 2002; 83 Oman et al., 2005; Sjolte et al., 2021). The downward propagation of the stratospheric polar vortex 84 anomaly into the troposphere can lead to regime shifts of the tropospheric Arctic Oscillation and 85 associated anomalous regional surface patterns (e.g., Zanchettin et al., 2012; Zambri et al., 2017). 86 In the case of polar vortex weakening, a critical role is attributed to increased likelihood of Sudden 87 Stratospheric Warming events (SSWs) (Haynes, 2005; Domeisen et al., 2020; Huang et al., 2021; 88 Kolstad et al., 2022, and references therein), whose projection on a negative Arctic Oscillation is expected to bring a series of consequences, including increased frequency of tropospheric 89 blockings and mid-latitude cold air outbreaks (e.g., Ma et al., 2024). However, the negative Arctic 90 91 Oscillation and associated tropospheric anomalies following SSWs are characterized by a low signal-to-noise ratio (e.g., Charlton-Perez et al. 2018; Zhang et al. 2019). Accordingly, recent 92 93 studies tend to disagree on this top-down mechanism being a robust dominant feature of climate 94 response to volcanic eruptions (Weierbach et al., 2023; DallaSanta and Polvani, 2023; Kolstad et 95 al., 2022; Azoulay et al., 2021; Polvani et al., 2019; Zanchettin et al., 2022; Toohey et al., 2014). 96 The radiative surface cooling following large volcanic eruptions has been shown to affect the 97 stratospheric polar vortex via a bottom-up mechanism (e.g., Graf et al., 2014; Peings and 98 Magnusdottir, 2015; Omrani et al., 2022). An example of this bottom-up mechanism following HL 99 eruptions is demonstrated in Sjolte et al. (2021) where they linked a weak polar vortex to an 100 increase in wave energy flux from the troposphere into the stratosphere without the meridional 101 stratospheric temperature gradient playing a major role. 102 With this in mind, the importance of transient atmospheric eddies (waves) and eddy-mean flow 103 interactions is becoming increasingly clear in explaining vertical and horizontal propagation of 104 atmospheric perturbations of various origins (e.g. Smith et al., 2022; Nakamura, 2023). DallaSanta 105 et al. (2019) used a hierarchy of simplified atmospheric models to show that eddy feedbacks are crucial in explaining stratosphere-troposphere coupling as well as the stratospheric response alone 106 107 following a tropical Pinatubo-like eruption. This demonstrates that the anomalous atmospheric 108 circulation response to an enhanced stratospheric sulfate aerosol layer cannot be understood as 109 the mere adjustment to meridional temperature gradients, and that eddy-mean flow interactions 110 and eddy feedback are an essential contribution to such response. Both mechanisms, i.e., the top-111 down mechanism triggered by local stratospheric heating and the bottom-up mechanism triggered

by surface cooling, act together in the real world and in realistic simulations. Therefore, idealized

112

Deleted: s

Deleted: s

Deleted: w

116 model experiments are required to assess their relative contribution to uncertainty in regional 117 climate variability during the period following the enhancement of the sulfate aerosol layer 118 (Zanchettin et al., 2016). 119 Jcelandic volcanism has played a role in shaping past NH climate variability and will continue 120 doing so. Two Icelandic eruptions during the past 2000 years, namely Eldgjá in ~939 CE and Laki 121 in 1783 CE, are considered to have had a significant impact on climate variability up to the global 122 scale (Brugnatelli and Tibaldi, 2020; Zambri et al., 2019; Oppenheimer et al., 2018; Thordarson 123 and Self, 2003; Stothers, 1998). These types of effusive eruptions are common in Iceland where 124 their duration can extend over years. During part of the eruption time such eruptions can become 125 explosive (referred to as mixed-phase eruptions) when ascending magma in a conduit comes in contact with water as was considered the case with both Eldgiá and Laki, explaining their 126 127 widespread impacts. Eruption history as well as dense monitoring network of Icelandic volcanic 128 systems tell us that many of these systems are currently on the verge of an eruption, having already 129 produced some of the largest volcanic eruptions over the past millennia (e.g., Öræfajökull, Bárðabunga and Hekla, Larsen & Guðmundsson, 2014; Barsotti et al., 2018; Einarsson, 2019). 130 131 Therefore history and current activity makes these types of eruptions an ideal reference case to 132 explore the potential climatic impacts of HL enhancements of the stratospheric sulfate aerosol 133 layer and to test hypotheses about the underlying mechanisms driving the climate response. This 134 is the focal point of this study where we investigate for the first time the role of wave-mean flow 135 interactions and SSWs in the climate response to a HL volcanic eruption. For this we perform 136 idealized, long-lasting HL volcanic perturbation experiments using the Community Earth System 137 Model version 1 (CESM1) in its coupled and atmosphere-standalone configurations. We evaluate the NH response during the first three winters following the eruption, referred to as post-eruption 138 139 winters in the text, and assess the dominating mechanism in each winter. This paper is organized as follows: Section 2 describes the model, experimental design and diagnostics; results are 140 141 presented in section 3 followed by discussions in section 4 where we end with concluding our 142 results in section 5.

Deleted: In the definition of a framework to study the climatic effects of a high-latitude enhancement of the stratospheric sulfate aerosol layer,

Deleted: provides for an ideal test bed, as it

Deleted: high-latitude

Deleted: atmospheric circulation

Deleted:

144 2 Methods

143

145

2.1. Numerical Model

We use the Community Earth System Model (CESM) version 1, developed by the National Center for Atmospheric Research (NCAR). In our configuration of CESM1, the atmospheric component is the Whole Atmosphere Community Climate Model, version 4 (WACCM4, Marsh et al. 2013). WACCM4 includes 66 vertical levels (up to 5.1×10-6 hPa, ~140 km) and uses CAM4 physics. We use the specified chemistry version of WACCM4 (SC-WACCM4), which is computationally less expensive to run, but simulates dynamical stratosphere-troposphere coupling and stratospheric variability like SSWs and the polar vortex with skills comparable to the interactive chemistry model version (Smith et al., 2014). CESM1/WACCM4 uses the Community Atmospheric Model Radiative Transfer (CAMRT) to parameterize the radiative forcing where it has been shown to accurately represent stratospheric aerosols by f. ex. simulating the temperature response following Mt. Pinatubo in 1991 (Neely et al., 2016). The SC-WACCM4 experiments are run with a horizontal resolution of 1.9° latitude by 2.5° longitude and include present-day (year 2000) radiative forcing. A repeating 28-month full cycle of the Quasi-biennial Oscillation (QBO) is included in the SC-WACCM4 experiments through nudging of the equatorial stratospheric winds to observed radiosonde data. In the coupled ocean-atmosphere configuration, the ocean component of CESM1 is the Parallel Ocean Program version 2 (POP2). CESM1 also includes the Los Alamos sea-ice model (CICE), the Community Land Model version 4 (CLM4) and the River Transport Model (RTM). CLM is run at a horizontal resolution of 1.9°x2.5°, POP2 and CICE are run at nominal 1° resolution with higher resolution near the equator than at the poles. Further details about CESM1 are given in Hurrell et al. (2013).

174 2.2. Volcanic Forcing File

153

154

155

156

157158

159

160161

162163

164

165

166

167168

169

170

171

172

173

175

176

177

178

179

180

182

183

We use the Easy Volcanic Aerosol (EVA) forcing generator (Toohey et al., 2016). EVA provides zonally symmetric stratospheric aerosol optical properties as a function of time, latitude, height, and wavelength (see detailed information on the tool in Toohey et al., 2016). EVA has been used to generate volcanic forcing in both idealized volcanic experiments (e.g., Zanchettin et al., 2016) and realistic paleoclimate simulations (Jungclaus et al., 2017) contributing to the sixth phase of the coupled model intercomparison project.

181 We use EVA to prescribe the volcanic aerosol loading corresponding to that of the 1991 Mt.

Pinatubo eruption (14.04 Tg SO₂), but at 45° N. Since the model reads the volcanic forcing as

aerosol mass mixing ratio (kg/kg) while our EVA output is in 1/m² (aerosol extinction), we scale

Formatted: Superscript

our forcing file by using the standard aerosol, input file for CAM4 and 5 (see Neely et al., 2016, Table 1) for the same eruption. A monthly scaling factor was derived from this linear relationship between the aerosol extinction and the aerosol mass mixing ratio that was used to scale the raw EVA forcing data (Fig. 1). From these scaled forcing data, the aerosol optical properties for our experiments are obtained with a two-step approach. First, we move the injection location northwards so that the center of the aerosol mass is at 65° N latitude and spans 10-28 km in altitude. Then, we define the start of the eruption to be May 1st and prolong the peak of the forcing by extending in time the highest monthly value in the so-obtained forcing data, so that the decline in aerosol mass begins 6 months after the start of the eruption or on November 1 (see Fig. 1). We thus obtain aerosol optical properties for an idealized, long-lasting high-latitude NH eruption. In this experiment we assume stratospheric injection only, although similar eruptions in the natural world would likely inject part of the total aerosol mass within the troposphere during the eruption. Past NH eruptions like Eldgjá and Laki had an atmospheric SO₂ loading of 219Tg and 122Tg respectively that was carried aloft with the eruptive column up into the upper troposphere with portions of the aerosols reaching the lower stratosphere during the eruptions (Thordarson et al., 2001). Hence our experiment can also be considered as a 6-month stratospheric aerosol injection that is analogous to similar although smaller eruptions (as compared to Laki) without the tropospheric aerosols.

184

185

186

187

188

189

190 191

192

193

194

195

196

197

198

199

200

201

202

203

204

205

206

207

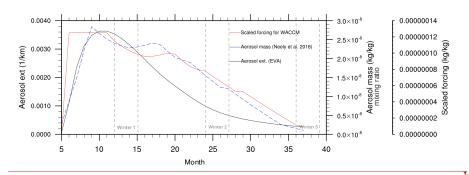
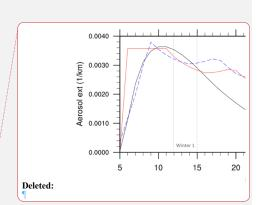


Figure 1: The time series of the original EVA aerosol extinction output (1/km, black curve) and the dry aerosol mass mixing ratio of the volcanic forcing file of Neely et al. (2016) (kg/kg, blue dashed curve) used for deriving the linear scaling coefficient for the conversion of EVA output into WACCM4 input (kg/kg, red curve). The horizontal axis is time (months) from the start of the

Deleted: mass

Deleted: (1/m²)
Deleted: (kg/kg)



eruption. Here we assume that the aerosol lifetime at 65° N is the same as at 45° N. Dashed vertical lines show the three winters that we focus on in this study.

216 **2.3.** E

213214

215

217218

219 220

221

222

223

224

225

226

227

228

229

230

231

232

233

234

235236

237238

239240

241

242 243

2.3. Experimental design

We ran two volcanic perturbation experiments with CESM1. The first experiment is conducted with the atmosphere-only version of the model, where boundaries to SC-WACCM4 are provided by prescribed fields of sea-surface temperature (SST) and sea-ice concentration (SIC) corresponding to the 1979-2008 monthly climatology of HadISST observations (Rayner et al., 2003). We refer to this experiment as *atm-only*. The second experiment is conducted with the coupled version of the model, henceforth referred to as *cpl*. For each experiment we run 20 ensemble members including the volcanic forcing and 20 paired ensemble members without the volcanic forcing and otherwise identical to the volcanic simulations, which we refer to as the control.

The atmosphere-only experiments were run over three full years, which provides two full winters after the onset of the eruption. We found that there was no need to extend the simulations further given the duration of the forcing and short memory of the atmosphere. The coupled experiments follow a similar protocol but they were integrated over 15 years to assess the response influenced by oceanic dynamical adjustment. However, in this study we only focus on the first three winters following the eruption, where the January and February forcing of winter 3 are defined to be a continuation of the December value of year 2. We define the first post-volcanic winter as December of the starting year (year 0) and the following January and February (year 1), the second postvolcanic winter is then December of year 1 and the following January and February of year 2 etc. Because the QBO is prescribed, and given its importance for the atmospheric circulation and the distribution of volcanic aerosols within the stratosphere (Thomas et al., 2009; DallaSanta et al., 2021; Brown et al., 2023), we have been careful in homogeneously sampling the QBO phasing that is imposed on the 20 ensemble members. For this, we shift the 28-month QBO cycle by one month for every ensemble member, so that the phasing of the QBO differs from one ensemble member to the next (Elsbury et al., 2021). This avoids potential biases in the climatic response that may be induced by any dominating QBO phase.

Deleted:

2.4. Diagnostics

245

246

247

248

249

250

251252

253

254

255

256

257

258

259

260

261

262

263

264

265

266

267

268

269270

271272

273

274 275 Model output is analyzed by computing paired anomalies, defined as deviations of each volcanic simulation from the corresponding control simulation (Zanchettin et al., 2022) (volcanic minus control). The statistical significance of the ensemble mean of paired anomalies is assessed at the 95% confidence interval, calculated from all 20 ensemble members, using a two-sided Student's ttest in addition to a Kolmogorov-Smirnov test.

To evaluate the effects of planetary waves on the zonally-averaged stratospheric response, we use the Eliassen Palm (EP) flux and its divergence (Edmon et al., 1980) in addition to the 3D generalization of the EP flux, the Plumb flux (Plumb, 1985), for a longitudinal representation in the lower troposphere and stratosphere. We identify SSW events by using an algorithm following the procedures described in Charlton and Polvani (2007), where mid-winter sudden warming events are determined to take place if the 10 hPa zonal-mean zonal wind at 60°N becomes easterly. Once a warming is identified, no day within 20 days of a central date, defined as the first day in which the daily mean zonal-mean wind at 60N and 10hPa is easterly, can be defined as an SSW. Changes in conditions for large-scale planetary waves propagation (waveguides) are examined using the optimal propagation diagnostic for stationary planetary waves, described in Karami et al. (2016). This metric is based on the construction of Probability Density Functions, for positive values of the refractive index (Matsuno 1970), as a function of zonal and meridional wave numbers. The refractive index is calculated using daily zonal wind and temperature at all levels, to derive monthly and zonally-averaged probabilities for stationary Rossby waves to propagate through the atmosphere, in function of latitude and pressure level. This is calculated for zonal wave numbers k=1,2,3 and meridional wave numbers l=1,2,3 (large-scale waves), and we average the probabilistic refractive index for each of the nine combinations of k and l, to provide a general estimate of chances for propagation of stationary planetary waves. For the eddy feedback calculations we compute the square of the local correlation across the ensemble members between DJF zonal-mean zonal wind and the divergence of the northward EP flux (delta phi F phi) averaged

over 600-200 hPa (Smith et al. 2022). In addition, we compute the rate of temperature (K) changes

in the 2m temperature (T2m) gradient using spherical harmonics to yield a T2m gradient in the

meridional (dZ/dlat) and zonal (dZ/dlon) directions.

Deleted: s

3 Results

In the following sections we will investigate the *cpl* experiment to characterize the forced response and identify the mechanism by utilizing the information provided by the *atm-only* experiment. We begin our investigation in the upper atmosphere before making our way towards the surface.

3.1. Volcanic radiative forcing

The net shortwave (SW) and longwave (LW) downward flux at the top of the atmosphere show an expected behavior following a stratospheric sulfate injection where we see a decrease in the SW due to scattering and an increase in the LW due to absorption around the injection location (Fig. 2c-f). Temporal perturbations of SW fluxes for both *cpl* and *atm-only* are influenced by the obvious strong seasonal evolution in solar insolation, where we see strong anomalies during the first summer north of 30° N than then becomes more confined to the mid latitudes as winter progresses with a slow decrease towards the end of the third year (Fig. 2c-d).

LW anomalies also show seasonal evolution with stronger LW flux at mid latitudes compared to at high latitudes during summer that continues into the winter season and remains significant throughout most of these three years. During winter, the LW anomalies are present at high latitudes where the SW anomalies are absent. The latitudinal bands of radiative flux anomalies correspond to the maximum values of the aerosol mass between 60 and 70° N, and the total aerosol mass of 14.04 Tg being largely confined north of 45° N (Fig. 2a-b). Overall, the idealized radiative forcing is largely bounded by the NH extratropics with the exception of a slight significant increase around 30-60° S in the second and third summer (Fig. 2c-d) that is visible at around 14-15 km a.s. (Fig. 2b). This occurs due to spatial features in the Neely et al. (2016) aerosol forcing that we use for scaling, where a slight aerosol increase occurs at lower latitudes, although this is not detectable when the aerosol mass is averaged through the atmospheric column with respect to time (Fig. 2a). We also detect a slight difference in the LW and SW fluxes that arises from differences in high cloud cover between *atm-only* and *cpl*, where *cpl* shows a decrease in high cloud cover in the northern high-latitudes, compared to *atm-only* (not shown).

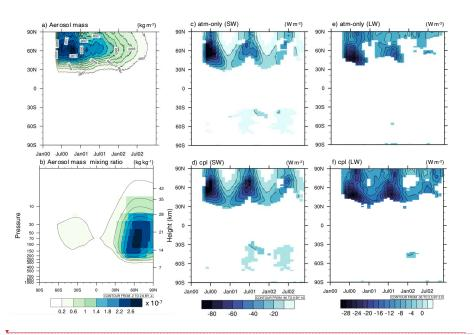
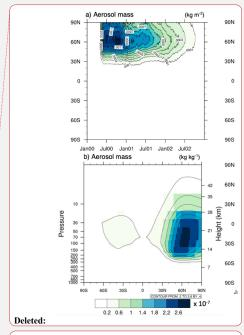


Figure 2: a) Average aerosol column mass time evolution in kg/m2 and b) pressure vs. latitude slice of the prescribed aerosol dry mass mixing ratio in kg/kg (3-year average). Aerosol mass is the same in cpl and atm-only. c) and d) show the time evolution of the net SW flux (downward) anomaly at the top of the atmosphere, and e) and f) the same but for net LW flux anomaly, resulting from the volcanic aerosol mass, in c) atm-only and d) cpl where coloured areas indicate 99% significance compared to the control experiment according to a Student's t-test.

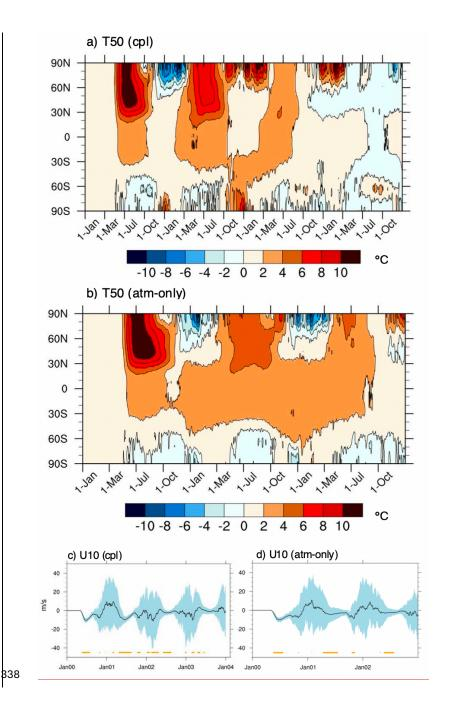
3.2. Stratospheric response

The strong seasonality in the LW perturbations described above also characterizes stratospheric temperatures, where a strong increase in the zonally averaged temperature at 50 hPa (T50) is detected north of 30° N during post-eruption summers in both experiments (Fig. 3a and 3b). This summer warming is followed by a net cooling of the polar stratosphere in the first winter seen for both *cpl* and *atm-only*. A clear difference in the T50 response in the two experiments is seen in winter 2, where *cpl* yields warming over polar latitudes while *atm-only* yields cooling (Fig. 3a,b). This reveals the intra-seasonal dynamical effects in the *cpl* experiment beyond the direct radiative



Deleted: Left panels:

response as we will see later on. The contrasting temperature response is accompanied by an opposite response in the zonal-mean zonal winds at 10hPa (U10) between 70 and 80° N. This U10 response is an indicator of the state of the polar vortex, where a polar vortex weakening is detected in winter 2 for *cpl* but a strengthening *atm-only* (Fig. 3c-d). Figures 3c-d do show a large ensemble spread in the zonal mean U10 winter response that is evident of a low signal to noise ratio. While the first winter in *cpl* and the first two in *atm-only* show little statistical significance according to a Kolmogorov-Smirnov test, this significance does increase for winter 2 in the *cpl* experiment. We also see this weakening in the zonal mean U50, also showing stronger significance during winter, (Supplementary Fig. S3) but not as clearly as in the zonal mean U10. However, for consistency we will mainly be focusing on the U50 response in the following section where this response is clear over the NH polar cap. The difference between *cpl* and *atm-only* will be in the focus in the following sections.



3.2.1 - First post-eruption winter

339

340

341

342

343

344

345

346 347

348

349

350

351

352

353

354

355

356

357

358

359

360

361

362

363

364

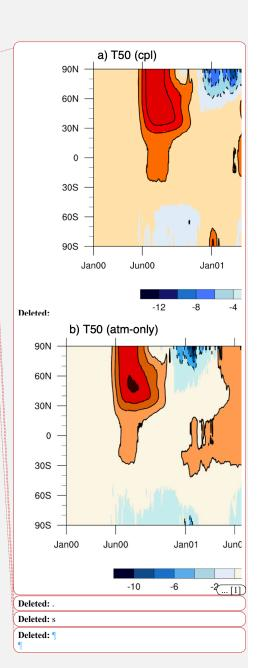
365

366

367

368

In the cpl experiment, the polar vortex strengthening in winter 1 is associated with extensive anomalies in temperature and zonal wind at 50 hPa (Fig. 4a). The anomalous temperature pattern consists of cooling at high latitudes and into the midlatitudes over the Atlantic, and warming over large swaths of the subtropics (to 20° N) and into the midlatitudes over the Pacific. This temperature pattern is also identified in the zonal mean T50 (Fig. 3b). Similarly, the zonal wind weakens into the midlatitudes over the Pacific while it is stronger in mid to high latitudes over the Atlantic. The strong upward EP flux (black arrows) is an indicator of the direction of propagated waves originating at the surface around the midlatitudes, where the horizontal and vertical EP flux components are proportional to the eddy momentum and heat flux, respectively (Fig. 4d). A convergence (negative divergence, dashed red contours) in the EP flux is detected in the upper troposphere that acts to weaken the tropospheric westerlies (Fig. 4d and Fig. S2). However, the EP flux and its convergence within the stratosphere does not appear to impact the stratospheric mean flow and the polar vortex. Therefore the local heating due to the volcanic aerosols and the associated increase in the meridional temperature gradient in the stratosphere appear to dominate the response of the polar vortex via thermal wind response, also depicted by the LW anomalies (Fig. 2f). Winter 1 in atm-only shows a similar thermal wind mechanism at play in the stratosphere as for the cpl experiment (Fig. 5a and 4a, respectively). In that case, less obvious tropospheric influences are detected, due to lack of forced surface cooling, as seen in the limited anomalous upward wave activity detected by the EP flux diagnostics (Fig. 5c).



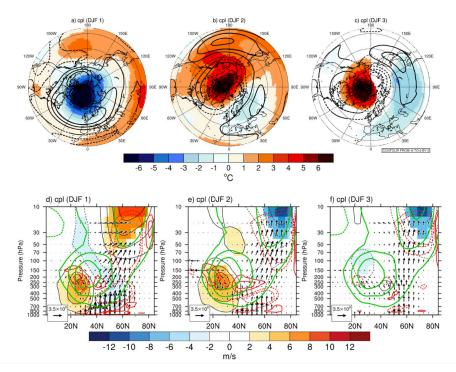


Figure 4: Winter stratospheric response in the *cpl* experiment. a-c) U50 (contours) and T50 (shading: red = warming, blue = cooling) response for winters 1-3, respectively. d-f) EP flux (arrows) and divergence (red contours) response, along with zonal-mean zonal wind response (black contours and shading: red = strengthening, blue = weakening) and climatology (green contours) in winters 1-3, respectively. Contours and color-shaded areas indicate 95% significance according to a Student's t-test. Only vectors that are significant at the 95% confidence interval are shown.

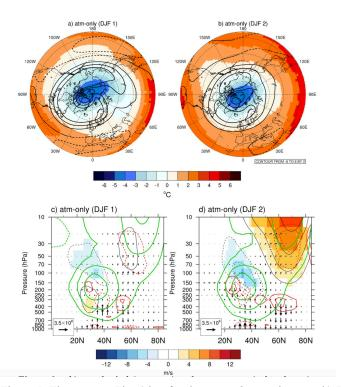


Figure 5: The same as Fig. 4 but for the *atm-only* experiment. a-b) Zonal wind (contours) and temperature (shading) response at 50 hPa for winter 1 and winter 2, respectively. c-d) EP flux (arrows) and divergence (red contours) response along with zonal-mean zonal wind (black contours) and pure climatology (green contours, 2m) in winters 1-2, respectively. Contours and colored area indicate 95% significance according to a Student's t-test.

3.2.2. Second post-eruption winter

A stark difference in the polar vortex response is detected between *cpl* and *atm-only* in winter 2. While *atm-only* exhibits a response similar to winter 1 (Fig. 5b), a significant warming over North America and the North Pacific emerges in *cpl* along with a weakening of U50 at high latitudes (Fig. 4b) indicating a shift of the polar vortex towards Eurasia. This warming at high latitudes then coincides with a slight LW absorption at high latitudes (Fig. 2f). The U50 weakening is not uniform throughout the longitudes explaining the lack of response detected in the zonal mean U50 (Fig.

- 402 S3), where one needs to go to U10 to get a clear response in the zonal-mean zonal wind (Fig. 3c).
- 403 An anomalously strong upward propagation of planetary waves persists in the cpl (Fig. 4e), with
- 404 a stronger upward EP flux now protruding into the stratosphere above 20hPa in contrast to winter
- 405 1. The upward EP flux and its convergence in the polar stratosphere are evident of their
- 406 contribution towards the weakening of the U50 and a general dominance over the effects of thermal
- 407 forcing by aerosols that have been, at this stage, substantially reduced (Fig. 1).
- 408 Similar wave propagation pattern as identified in the cpl experiment is known to be associated
- 409 with SSWs. We suspect that the decrease in the T50 difference between mid- and high latitudes
- 410 can act as a trigger for a weaker polar vortex in addition to the stratosphere absorbing the upward
- 411 propagating waves that is known to cause warming over the polar cap (Kodera et al., 2016;
- 412 Kretschmer et al., 2018). We will see further evidence of this in the next section.

3.2.3. Third post-eruption winter

413 414

- 415 The results in this section only refer to the *cpl* experiment since winter 3 is lacking in *atm-only*.
- 416 The SSW-like pattern of winter 2 clearly continues into winter 3, where most of the volcanic
- 417 aerosols have decreased to the extent that their radiative impacts no longer dominate. An exception
- 418 is the confinement of T50 warming over the polar stratosphere (Fig. 4c). Furthermore, anomalous
- 419 upward propagation of planetary waves continues to persist (Fig. 4f). This upward wave flux in
- 420 addition to the T50 warming resembles a pattern that behaves much like absorbing SSWs defined
- 421 by Kodera et al. (2016). To examine this response further we define SSWs based on the reversal
- 422 of the zonal-mean zonal winds at 60° N and at 10hPa between November and March according to
- 423 the method of Charlton and Polvani (2007).
- 425 Results from the SSW analysis are presented in Fig. 6. No significant increase in SSWs is found
- 426 in winter 2, despite the SSW-like pattern detected. This changes in winter 3 when the difference
- 427 between perturbed and unperturbed experiment becomes statistically significant, with 27 SSWs
- 428 occurring in our forced experiment compared to only 6 in the control experiment. This increase in
- 429 SSWs agrees well with the U50 and T50 anomalies of winter 3 (Fig. 4c). During winter 2, the
- 430 warming of the polar stratosphere is as strong as in winter 3 but more spread out into midlatitudes.
- 431 These results are also in agreement with the stratospheric Plumb flux in winter 3 (Fig. S1c) where

the upward flux is mostly circumpolar between 40° and 60° N, showing further evidence of the SSWs detected.

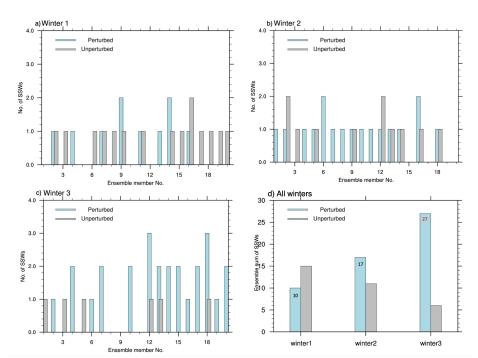


Figure 6: a-c) The number of SSWs during winters 1-3 for each ensemble member in the *cpl* experiment and d) The sum of all SSWs in each experiment for all 20 ensemble members of winters 1-3 both for *cpl* (light-blue bars) and control (gray bars). The color red indicates 95% significance according to a two-sided Student's t test.

When comparing the ensemble sum of SSWs in the perturbed and unperturbed experiment using a Kolmogorov-Smirnov test (Fig. 6d), a significant increase in the number of SSWs occurs in winter 3 (p=0.0135). This underlines the generally strong SSW response occurring in winter 3, when the fraction of ensemble members having more than 1 SSW per winter increases to 50% (10 ensemble members) in winter 3 compared to only 10% in winters 1-2. Of these 10 ensemble members, two members show three SSWs per winter that can be considered highly unlikely based

Deleted: 5

on historical records. Although winters with more than 1 SSWs are considered unusual, examples do exist in the observational record of multiple SSWs in one winter, like the winter of 1998/1999 and 2009/2010 (Kodera et al., 2016 and Ineson et al., 2023 respectively).

448

449

450

451

452

453

454

455

456

457

458

459

460

461

462

463

464

465

466

467

468

469

470

471

472 473

474

475

476

477

478

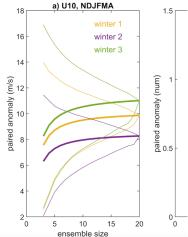
To better understand the cpl SSWs response, we also did an SSW analysis on *atm-only* (Fig. S7) where 50-75% less SSWs were detected in the perturbed simulation compared to the unperturbed one. Such a response should not be unexpected during the forced polar vortex strengthening as detected in *atm-only* (see Fig. 5). Furthermore, only single SSWs per winter were detected in all 20 ensemble members of the perturbed simulation while two (one) ensemble member(s) detected double SSWs per winter 1 (winter 2) in the unperturbed simulation. Although these results do suggest an increase in the number of SSWs in the *cpl* simulation, internal variability is large and the frequency of SSWs fluctuates substantially between the three winters in the unperturbed simulation.

We explored the impact of the ensemble size for the ensemble spread of two key diagnostics of our mechanism, namely U10 and SSW, calculated as the standard deviation of post-eruption paired anomalies for the first three post-eruption winters (Supplementary Fig. S8). Winter 3 produces larger spread than winters 1 and 2, indicative of a least constrained forced response, which is especially evident for ensemble sizes larger than 15. Therefore, only much larger ensembles may provide signals not encompassing the value of zero within uncertainty.

According to the above, the evolution in *cpl* from winter 1 to winter 3 can be summarized as follows: In the first winter, the thermal forcing appears to be stronger than the upward wave flux because of the large amount of aerosols present, thereby dominating the response that causes the polar vortex strengthening and the inclusion of cold polar air within. In the second winter, the thermal forcing from the volcanic aerosols at midlatitudes has decreased where it is now mostly confined to higher latitudes as seen both in the LW flux and T50 (Fig. 2f and Fig. 3b). We suspect that in addition to the aerosol decrease, this slight decrease in the temperature difference between high and midlatitudes allows the strong upward wave flux to dominate and enter the upper stratosphere. There in the stratosphere, the waves are absorbed that causes further warming over the polar cap in addition to weakening the zonal stratospheric winds (Fig. 5b and Fig. 4b). This upward wave flux and weaker winds continue into the third winter, where winter 2 potentially acts as a precursor, allowing for SSWs to develop more frequently as detected in the T50 warming that

Deleted: show strong evidence of

Deleted: Since this is indicative of a low signal-to-noise ratio and uncertainties in the response of polar vortex variability, we tested the potential impact of ensemble size on the signalto-noise ratio for two key diagnostics of our mechanism, namely U10 and SSW. We express the signal-to-noise ratio as the uncertainty related to the expected (i.e., ensemble mean) response, calculated as standard error of the mean of posteruption paired anomalies for the first three post-eruption winters. The standard errors converge toward the value obtained for the full 20-member ensemble for all winters and both variables (Figure 7), with a common tendency of growing uncertainty in the expected response with the ensemble size. The mean curves consistently level off for ensemble sizes larger than 10, suggesting that the full ensemble estimate is representative of uncertainty in the expected response for larger ensemble sizes. Otherwise, winter 3 produces larger uncertainty than winters 1 and 2, suggesting a less constrained forced response. This is especially evident for estimates of standard error of SSW anomalies and ensemble sizes larger than 15, where winters 1 and 2 closely superpose on each other while winter 3 does not overlap with winters 1 and 2 within the 5-95th percentile range. Overall, the flattening of the ensemble-mean expectations on the standard error, and the large values diagnosed in winter 3, suggest that the winter 3 response features an intrinsically lower signal-to-noise ratio. In fact, since the value of full-ensemble mean SSW paired anomaly in winter 3 (+1.05 events) is similar to the associated expected standard error (+1.02 events) we conclude that even a much larger ensemble would not provide more certainty in the signal detected. ..



Deleted: ensemble size Figure 7: Impacts of ensemble size and spread on the volcanic signal. Ensemble mean (thick lines) and associated standard errors (thin lines, 5-95 percentile range) of paired anomalies calculated for different ensemble sizes and for the first (...[2])

Deleted: likely

is now confined over the polar cap (Fig. 4c and Fig. 5c, respectively). The SSW development is also evident in both U10 and U50 and T50 timeseries (Fig. 3c and Figure S3a-b respectively), where peak T50 warming occurs late in winter 3. The expected absence of a surface response is obvious in our atm-only experiment where basic physical mechanism, via the thermal wind balance due to radiative heating, dominates the atmospheric circulation response in the first two posteruption winters. The strong stratospheric polar vortex then isolates the cold air over the polar regions (Fig. 5a-b) as is the case in winter 1 of in the cpl experiment (Fig. 4a).

Deleted: , with a
Deleted: ing

Deleted: in the second winter

Deleted: (Fig. 5a-b)

3.3. Tropospheric response

What is it then that drives this polar vortex weakening and the SSW response in the *cpl* experiment? To examine in more detail the origin of the upward wave fluxes in winters 2 and 3 of the *cpl* experiment that causes the detected polar vortex weakening and the SSWs, we now turn our attention towards the troposphere.

We begin by comparing the response of T2m, vertical Plumb flux at 850 hPa and 200 hPa zonal wind, in *cpl* (Fig. 7) and in *atm-only* (Fig. 8).

As a response to the decrease in SW flux following the eruption, extensive and heterogeneous cooling is identified in the T2m anomalies in winters 1-3 (*1-2 for atm-only*) over latitude bands that contain the most significant SW flux decrease (Fig. 2d, Fig. 7a-c and Fig. 8a-b). The strongest cooling occurs over northeastern North America and along the Asian midlatitudes in winter 1, with much larger amplitude in *cpl* than in *atm-only* (Fig. 7a versus Fig. 8a). In *cpl*, a significant cooling is identified in the SST (Fig. S5), extending the area of negative T2m anomalies towards the ocean, in particular over the northwestern North Pacific in winter 1 (Fig. 7a). There it progresses from an initial preferential surface cooling over the midlatitudes in winter 1 to a later cooling of polar regions in winter 3 (Fig. 7c). In *atm-only*, the surface response is hampered over the ocean by the experimental design, and T2m anomalies are therefore confined to landmasses, yielding an overall much weaker temperature response compared to *cpl* (Fig. 8a-b).

Deleted: 8

Deleted: 9

Deleted: 8

Deleted: 9

Deleted: 8
Deleted: 9

Deleted: significantly cools down

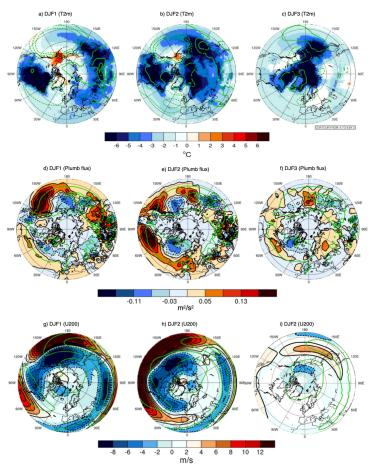
Deleted: which extends

Deleted: over

Deleted: 8
Deleted: 8

Deleted: 9

Deleted: ¶



578

579

580

581

582

583

Figure 7, a-c),2-meter air temperature (°C) in *cpl* (color) and sea-level pressure (green contours) anomalies for winters 1-3. d-f). The vertical component of the Plumb flux (m²/s²) at 850 hPa in *cpl*, and the climatology as green contours from -8 to 12 by 2, for winters 1-3. g-i),200 hPa zonal wind (m/s) anomalies in *cpl*, and the climatology as green contours from -0.15 to 0.15 by 0.04, for winters 1-3. Contours and colored areas indicate significance at the 95% confidence interval according to a Student's t-test.

Deleted: 8

Deleted: a) Response of

Deleted:

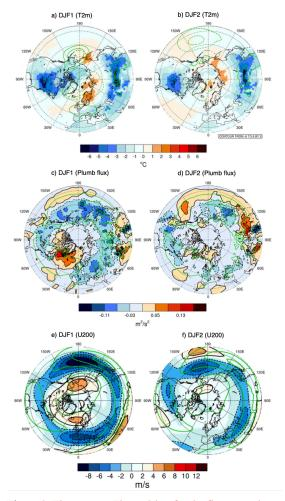
Deleted: ,

Deleted: b) Same as *a)* but for winter 2. c) Same as *a)* but for winter 3. d) Response of

Deleted: 850 hPa

Deleted: e) Same as *d)* but for winter 2. f) Same as *d)* but for winter 3. g) Response of

Deleted: h) Same as g) but for winter 2. i) Same as g) but for winter 3.



597

Figure & The same as Figure 8 but for the first two winters in atm-only. Contours and shaded areas indicate significance at the 95% confidence interval according to a Student's t-test.

Deleted: 9

Deleted: a) Response of 2-meter air temperature (°C) in *atm-only*, and sea-level pressure (green contours), for winter 1. b) Same as *a*) but for winter 2. c) Response of 850 hPa vertical component of the Plumb flux (m²/s²) in *atm-only*, and the climatology as green contours from -8 to 12 by 2, for winter 1. d) Same as *c*) but for winter 2. c) Response of 200 hPa zonal wind (m/s) in *atm-only*, and the climatology as green contours from -0.15 to 0.15 by 0.04, for winter 1. f) Same as *e*) but for winter 2.

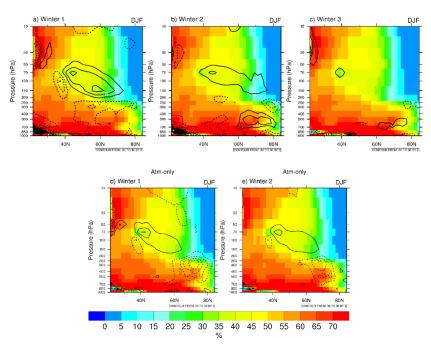


Figure 9 Probability (%) of favorable propagation conditions for large-scale stationary Rossby waves (zonal and meridional wavenumbers 1, 2 and 3) as a function of latitude and pressure levels (shading). Contours show the response in long_summer versus control. a) Winter 1 in *cpl*. b) Winter 2 in *cpl*. c) Winter 3 in *cpl*. d) Winter 1 in *atm-only*. e) Winter 2 in *atm-only*.

The vertical component of the the Plumb flux at 850 hPa (Fig. 7d-f) allows us to locate the origins of the upward EP flux in *cpl* (Fig. 4d-f). It is strongest over the north eastern part of the Pacific Ocean (off the west coast of North America) in winter 1, where it continues up into the lower stratosphere at 150 hPa (see Fig. S1a). In winter 2, the Plumb flux has decreased in the North Pacific and increased over the North Atlantic and Siberia, pointing to a possible influence of the change in land-sea temperature contrast (Fig. 7e). In addition to this upward flux, we also detect downward wave flux over both the Aleutian and Greenland regions at 850 hPa and over a large area south of 45° N at 150 hPa (Figure S1b). This downward Plumb flux is evidence of changes in the planetary wave structure where wave reflection occurs due to the sudden weakening of the zonal winds identified in the U10 (Fig. 3a). In winter 3, the Plumb flux now dominates both at 850

Deleted: 10

Deleted: 8

Deleted: 8

(seen in Fig. 7f) and 150 hPa (Fig. S1c), where it encircles the polar stratosphere north of 60° N. In line with the weak EP-flux response shown in Fig. 5, the Plumb flux anomalies are generally weak in *atm-only* compared to *cpl*, for both winter 1 and 2 (Fig. &c-d).

627

628

629

630 631

632

633

634

635

636

637 638

639

640

641

642

643

644

645

646

647

648

649

650

651

652

653

654

655

656

657

Since upward wave activity depends on wave-mean flow interactions, several factors are at play to explain the strong response in cpl vs atm-only. First, the change in zonal flow is substantially different between the two pairs of experiments, as shown by the U200 anomalies (Fig. 7g-i and Fig. Se-f). In the first two winters we observe an intense deepening of the Aleutian low in cpl (Fig. 7a-b) associated with a large equatorward shift of the subtropical jet over the North Pacific (Fig. 7g-h, also seen in the zonal-mean averages of Fig. 4). The change in zonal flow is not as large in atm-only, where there is a general decrease of U200 on the poleward side of the subtropical jets, rather than a marked equatorward shift as in cpl. This further emphasizes that amplified surface coupling when the ocean is coupled to the atmosphere has a dramatic impact on the amplitude of the tropospheric response. Because the zonal flow acts as a waveguide for large-scale planetary waves, we expect changes in upward wave propagation in the stratosphere. To measure how waveguides change, we compute the probability of favorable propagation conditions for largescale stationary waves (Fig. 9). This is averaged for zonal wave numbers k=1,2,3 and meridional wave numbers l=1,2,3, as a function of pressure and latitude (see section 2 for more details). Areas of high probability show where large-scale waves preferentially propagate, while low probability regions indicate where linear wave propagation is hampered. Generally, the mid-latitude troposphere is more favorable for wave propagation than the high-latitudes and the stratosphere, consistent with the tendency for stationary waves to propagate upwards and to be deflected towards the equator, in climatology. After injection of the volcanic forcing, both cpl and atm-only exhibit an increase in the probability for wave propagation between 40 and 60 °N in the lower stratosphere during winter 1 and 2, but the responses in the troposphere are markedly different. In atm-only, wave propagation is inhibited in the free troposphere north of 60°N, for both winters 1 and 2 (Fig. 2d-e), which is consistent with the EP-flux anomalies of Fig. 5. This response is absent from cpl during winter 1 (Fig. 2a), and opposite during winter 2 when an increase of favorable conditions for wave propagation is diagnosed (Fig. 9b). We also see that the waveguide has greatly reduced in the subtropical troposphere in cpl winters 1-2 that favor large-scale waves to be redirected towards the pole. This increase in favorable conditions for wave propagation in the troposphere Deleted: 8

Deleted: 9

Deleted: 8

Deleted: 9

Deleted: 8

Deleted: 8

Deleted: Fig. 10 shows

Deleted:

Deleted: 10

Deleted: 10

Deleted: 10

between 60 and 80 °N persists during winter 3 in *cpl* (Fig. 9c), which is a partial and the most likely explanation for enhanced upward wave propagation in the stratosphere described in Fig. 4f.

671672673

674

675

676

677

678

679

680

681

682

683

684

685

686

687

688

689

690

691

692

693 694

695

696 697

698

699

669

670

In cpl winter 3, when the cooling is reduced in the NH mid-latitudes and has migrated towards the polar regions (also evident in SST, see Fig. 5S), the amplitude of the 850 hPa upward Plumb flux anomalies decreases compared to previous winters (Fig. 7f). This suggests that the mid-latitude spatiotemporal cooling pattern plays a part in the strong wave activity detected near the surface. This can be revealed by computing the T2m gradient (Tgrad) where strong land-sea temperature gradients are known for their ability to influence atmospheric wave activity (Hoskins and Valdes, 1990; Brayshaw et al., 2009; He et al., 2014; Wake et al., 2014; Portal et al., 2022). Figure 10a shows sharp significant changes in the meridional gradient that encircles 45° N in winter 1, with positive (negative) gradient anomalies occurring south (north) of 45° N. In winter 2 we still see the gradient present at 45° N but now located over North America and the North Pacific. Winter 3 mostly reveals regional anomalies in the Barents-Kara, Greenland-Iceland and the North Pacific regions (Figure 10b-c), occurring over areas of significant sea ice increase (not shown). The sharp Tgrad change in winter 1 (Fig. 10a) is followed by a reduction of land-sea temperature contrast over eastern Canada and the U.S. in winter 2 (Fig. 10b). This is a known cause of planetary wave enhancement (Portal et al., 2022) and could provide an explanation for the strong surface upward wave flux detected in the second and third post-volcanic winters (Figure 7e-f). Both the zonal and meridional Tgrad components show an increase in the northern part of Alaska that coincides with the region of T2m warming over the Aleutian/Alaska region (Fig. 7a) and the strong upward Plumb flux (Fig. 7d). This warming, in addition to the strong continental cooling over North East America and the general decrease in Tgrad spanning from mid to northern part of North America, might influence this strong Plumb flux anomaly in the North Pacific. Of note, sea-ice extent increases around East Siberia extending into the Chukchi Sea (not shown), highlighting the potential influence of sea ice variability on Tgrad and upward Plumb flux anomalies in the area.

Plotting the average Tgrad for various regions against the average number of SSWs for winters 1-

3 (Fig. S6), we do see that the strongest Tgrad reduction occurs over the North East US in the

second winter. This is in agreement with the upward Plumb flux over the same region and serving

as further evidence for its contribution to the upward EP flux in winter 2. This Tgrad reduction

Deleted: 10

Deleted: , which is

Deleted: the

Deleted: (

Deleted: 8

Deleted: In winter 1 the meridional gradient

Deleted: ing

Deleted: (Fig. 11a)

Deleted: 11 Deleted: A

Deleted: throughout the NH at 45° N is identified

Deleted: 11
Deleted: that

Deleted: 11

Deleted: 8

Deleted: 8
Deleted: 8

Deleted: .

Deleted: ing

719 co 720 th 721 co 722 S

723

724

725 726

727

728

729 730

731

732

733734

735

continues into the third winter where we also detected a reduction in the upward Plumb flux over the same area (Fig. 7f). Looking towards the Barents Sea, a clear spatial difference emerges compared to the North East US, where a clear Tgrad increase occurs in winter 3 related to the SSWs. In general less changes are detected between winters in the North West NA and the North Pacific, reflecting the confined cooling over higher latitudes in winter 3 associated with the SSWs.

Deleted: 8

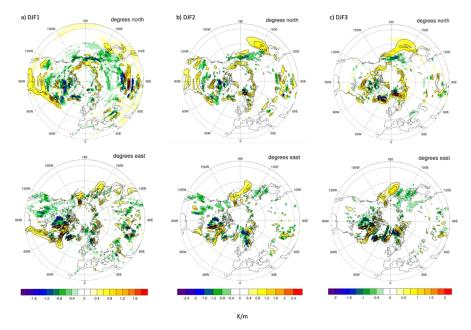


Figure 10; a-c) The zonal (degrees north) and meridional (degrees east) T2m gradient anomalies (perturbed minus unperturbed) for winters 1-3. Contours indicate 95% significance according to a Student's t-test. Note the different colorbar for each winter.

To complete our assessment of the tropospheric response, we examine if eddies play a role in the *cpl* polar vortex response and the anomalous upward EP flux (Fig. 4a-f) as well as SSWs detected in winter 3 by following Smith et al. (2022) (see Methods). This is done for both perturbed (red) and unperturbed (blue) experiments in *cpl* and *atm-only* (Fig. S4). We see an increase in perturbed eddy feedback at around 40-70° N both for *cpl* winter 1 and winters 1-2 in *atm-only* during the polar vortex strengthening (Fig. S4). However, the role of eddies in the polar vortex weakening in

Deleted: 10

winters 2-3 is unclear, especially considering the eddy feedback increase of the control run in winter 2 (Fig. S4b). In general, these results suggest that the signal-to-noise ratio is too small to identify a role for eddy feedback in our experiments.

738

739

740

741 742

743

744745

746

747

748

749

750

751

752753

754

755

756 757

758

759

760

761

762

763

764

765

766

767

768

4 Discussion

Our two sets of coupled ocean-atmosphere (cpl) and atmosphere-only (atm-only) experiments examine the large-scale climate response to an idealized long-lasting NH eruption, where their differences give us valuable insight into the volcanically forced mechanisms at play within the coupled climate system in CESM1. Specifically, we analyzed the first three winters of the cpl experiment and used the first two winters of atm-only as a comparison to investigate the dynamics that govern the post-eruption stratospheric polar vortex and the associated surface response.

Results from the cpl experiment show a similar response in the first winter as in the two winters of atm-only, with a strengthening of the zonal winds resulting from an aerosol-induced sharp temperature gradient between the mid-latitudes and the pole (Fig. 4a and Fig. 5a). We show that this zonal wind strengthening is not affected by the detected strong upward EP flux, where the LW flux (Fig. 2e-f) supports our conclusions that the polar vortex strengthening is induced by the thermal wind balance. A distinct change to this pattern emerges in cpl winter 2 where we detect an SSW-like pattern, with strong negative anomalies emerging in the polar U50 winds and a warming in the T50 field (Fig. 4b). We also detect an LW absorption at high latitudes, that is absent at midlatitudes, where this T50 warming is evident of the potential role of a decreased temperature gradient in the identified polar vortex weakening. Furthermore, the upward wave-activity flux from the troposphere into the stratosphere and the T50 warming indicate absorption of upward propagating waves into the stratosphere that causes this warming and weakening of U10 winds over the polar cap. This pattern is known to be related to SSWs (Kretschmer et al., 2018; Kodera et al., 2016), agreeing with our results in winter 3 where an increase in the occurrence of SSWs is detected. The strong upward EP flux greatly depends on ocean-atmosphere coupling originating in the surface cooling in addition to the changes in upper tropospheric zonal flow. This further contributes to the upward EP flux from the troposphere into the stratosphere that eventually leads

Although the above coincides with a positive (negative) eddy feedback in the first (second) winter that could in theory play a role in sustaining the strengthening (weakening) of the polar vortex, our

to polar vortex weakening and enhanced SSWs.

Deleted: that we further confirm

Deleted: to occurr

eddy feedback results indicate low signal-to-noise ratio where further studies with additional ensemble members would be required to confirm their role in the forced response. We also note that Smith et al. (2022) identified CESM1 WACCM-SC as having one of the weakest eddy feedback of the sixteen models they investigated, so the response of eddy feedback may be more significant in other models. Similar to the eddy feedback, low signal-to-noise ratio is also evident in the SSW analysis. However, the response we detect in the U50 and T50 fields is strong compared to the unperturbed simulation where the SSWs provide an explanation in agreement with the patterns detected. Furthermore, the SSW analysis for atm-only and the ensemble size test (Fig. S7 and Fig. S8 respectively) both show strong evidence of a robust signal for winter 3 despite the noisy polar vortex and the limited ensemble size. We also see that the large decrease in SSWs in the perturbed simulation of atm-only (when compared to unperturbed) is consistent with the detected polar vortex strengthening. This further supports the significance of the signal we detect in cpl winter 3 compared to the background noise. In addition, all winters examined, in both cpl and atm-only, showed that there is up to 15% chance of getting more than 1 SSWs per winter in all ensemble members. This is not far from Ineson et al. (2022) who identified a double event once every 9 years in a 66-year ERA5 record. The exception is cpl winter 3 that is also the only winter that has 3 SSWs, with the average SSW occurrence also being the only winter above 1 (1.17) while all other winters span between 0.15-0.85 per winter. A similar NH high-latitude eruption has not taken place during the observational period, so we have no comparison. Also, to the best of our knowledge, a similar high-latitude sulfur injection study has not been performed before. Therefore, it is difficult to say at this stage if such a response is realistic or not, but in general more than two SSWs per winter can be considered exceptional yet plausible, as is also the case for our idealized eruption.

793 794 795

796

797

798

799

800

771

772

773 774

775

776

777

778

779

780

781

782

783

784

785

786

787

788

789

790

791

792

Bittner et al. (2016b) identified an opposite response driven by a similar underlying mechanism, when compared to our *cpl* response in winters 2-3 (Fig. 4), following a Tambora-like eruption where a strengthening of the polar vortex due to less wave breaking at high latitudes was considered to be an indirect effect associated with a changes in planetary wave propagation. Since the volcanic aerosols in our experiments have declined extensively in the third winter, making the aerosol thermal forcing a limited factor, we cannot rule out similar indirect effects where changes

Deleted: 7

Deleted: b

in wave propagation leads to an increase in wave breaking at high latitudes and hence the increase in SSWs.

While not directly comparable to our study but still providing an important analog, Muthers et al. (2016) identified an average increase in the number of SSWs during a 30-year (constant) decrease in solar radiation in line with our significant increase in SSWs in winter 3. Our results do support the findings of Sjolte et al. (2019), where the stratospheric temperature gradient does not appear to play a major role in the polar vortex weakening we identify, while the upward wave flux does. The strong surface cooling detected in Fig. 7 is a well-known caveat in CMIP5 models (including CESM1) (Driscoll et al., 2012; Chylek et al., 2020) and is clearly detected in our coupled simulations. Since our results indicate the dominant role of the volcanically induced stratospheric thermal wind response that causes the polar vortex strengthening, the cooling does not appear to impact the response identified in winter 1. This is also revealed by the EP flux. The same cannot be said about winters 2-3, where our results indicate that the exaggerated spatiotemporal T2m pattern might explain the strong upward wave flux and the associated stratospheric response. Interestingly, a slight difference between *atm-only* and *cpl* is detected in both the LW and SW flux that is caused by a strong significant decrease in high cloud cover in the *cpl* simulation (not shown). This cloud cover decrease, especially at mid- to high latitudes, agrees with the increased LW fluxes

at higher latitudes in addition to the decrease in SW flux and the associated surface cooling. This

raises a question regarding the role of forced surface processes in these high cloud changes, which

we leave open for further studies.

As mentioned in the methods section, we assume a similar lifetime of volcanic aerosols at 65° N as at 45° N. When considering the e-folding time in Toohey et al. (2019), a substantial aerosol decrease of about 43% occurs at 17km (a.b.s.) for an eruption at 60° compared to at 0°. However, since our experiment assumes a constant stratospheric injection over 5 months with the aim to simulate a long-lasting HL eruption compared to a single injection at low latitudes, the difference in the e-folding time between low and high-latitudes would be expected to decrease. Using CESM2-WACCM6 with interactive chemistry Zhuo et al. (2023) identified that although an eruption at 64° N did have a shorter aerosol lifetime compared to one at 15° N, it leads to stronger volcanic forcing over the NH extratropics. In addition, one of their conclusions was that different duration and intensity of both tropical and NH extratropical eruptions can lead to different results,

Deleted: 8

stressing that our 6 month long stratospheric sulfate aerosol enhancement is not directly comparable with volcanic eruptions of shorter duration. Although the aerosol lifetime in our experiment might be exaggerated into the third year, our results do indicate that the polar vortex weakening in winter 2 appears to act as a trigger for further weakening that eventually leads to SSWs in winter 3. In order to increase confidence on such a delayed link, additional sensitivity simulations are required, which we we leave that for future studies.

835

836

837

838

839

840

841 842

843 844

845

846

847

848

849

850

851

852

853

854

855

856

857

858

859 860

861

862 863

864

865

Deleted: precu

Unlike our eruption simulated using a version of WACCM4, where the chemistry is prescribed, natural volcanic eruptions can contain various chemical compounds that impact the formation and the lifetime of sulfate aerosols as well as affect the atmospheric circulation via, e.g., ozone depletion, like halogens are known to do. More advanced versions as well as models that include interactive chemistry are thus important to reveal in more detail the chemistry-climate interactions that occur in the natural world (Clyne et al., 2021; Case et al., 2023; Fuglestvedt et al., 2024). Thus our idealized experiment can be considered primitive in the sense that it only considers sulfate aerosols but sufficient when focusing on answering questions on the basic mechanism that such eruptions can initiate. Another important aspect that we do not focus on in our study is the role of different initial conditions on the forced climate response, where initial atmospheric and climate conditions, including e.g. the stability of the polar vortex, control the lifetime and distribution of the volcanic aerosols as well as the forced dynamic climate response (Zanchettin et al., 2019; Weierbach et al., 2023; Zhuo et al., 2023; Fuglestvedt et al., 2024). An exception is our assessment on how the easterly and westerly phase of the QBO affect our results where we compared ensemble members showing easterly phase with the westerly ones to test if the U50 and T50 response patterns would be different. They were not: both phases showed a weakening of the U50 although the zonal winds were more confined and consistent over the higher latitudes of the NH during the easterly phase (not shown). The difference in the number of ensemble members used for these calculations could of course impact the statistics of this test of ours but not the overall pattern detected.

CESM2-WACCM6 has obvious improvements when compared to CESM1-WACCM4 (see e.g. Gettleman et al., 2019, Danabasoglu et al., 2020), among them being an interactive QBO as well as having a slightly higher frequency of SSW occurrence (Holland et al., 2024). Nonetheless, CESM1-WACCM4 has comparable transient climate response to CESM2 as well as the ability to

capture the general physical mechanism occurring within the climate system as identified in various recent studies (Danabasoglu et al., 2020; Zang et al., 2018; Elsbury et al., 2021b; Peings et al., 2023; Ding et al., 2023; Yu et al., 2024).

870 871

869

867 868

5 Conclusions

- Through comparison of the *cpl* and *atm-only* simulations, our results clearly demonstrates the important role of ocean-atmosphere coupling in the stratospheric response to enhancements of the stratospheric sulfate aerosol layer at higher NH latitudes. We see that this aerosol enhancement
- layer triggers two competing mechanisms in the first three winters:
- 876 i) Winter 1: The stratospheric polar vortex strengthening is triggered by stratospheric aerosol
- 877 thermal forcing via thermal wind balance. This response is not influenced by the strong upward
- 878 wave flux identified, originating in the forced surface cooling and changes in tropospheric
- 879 circulation, and provides strong evidence of two mechanisms that are competing simultaneously:
- 880 A Top-down and a Bottom-up mechanism, where the Top-down mechanism dominates the
- 881 response.
- 882 ii) Winter 2: The upward wave flux is absorbed in the stratosphere that causes a warming over the
- 883 polar cap and a polar vortex weakening. This pattern is similar to SSWs although its occurrence is
- 884 not significant. Here the Bottom-up mechanism dominates.
- 885 iii) Winter 3: The persistence of the upward wave flux continuing into the third winter leads to an
- 886 increase in SSWs with warming now confined over the polar cap, again demonstrating the
- dominating Bottom-up mechanism as in winter 2.
- 888 It is clear from our results that the strong surface cooling following the HL sulphate aerosol
- 889 injection causes dramatic changes in tropospheric circulation. These changes further modify
- 890 atmospheric waveguides where we detect an increase in propagation of planetary waves in the
- 891 lower stratosphere occurring at higher latitudes. Although we do find similarities in the eddy
- 892 feedback when compared to the general climate signal that we identify, such as the decrease in
- 893 eddy feedback in winter 1 potentially sustaining the polar vortex strengthening, we emphasize its
- weak signal. At the same time we encourage further studies on this subject, especially concerning
- 895 the lack of published comparison studies regarding both high and low latitude volcanic eruptions
- 896 and SSWs. Ideally such studies would include the latest model generations in addition to
- 897 observational datasets. They should also consider the impact of different climate realizations and

the eruption magnitude on the forced response. Furthermore, these results highlight the importance of including high-latitude volcanic forcing simulations of various lengths and/or magnitudes in projects such as VolMIP, especially considering the current volcanic unrest and increased activity in some of the major volcanic systems in Iceland.

Data availability

The model output is available upon request by contacting the corresponding author.

Author contribution

HG conceptualized this study along with GM, YP and DZ. *cpl* and *atm-only* experiments were carried out by HG and YP. Analysis and calculations of model output as well as graphical representation was done by HG except for the eddy feedback and the probability of favorable propagation conditions that was done by YP and the ensemble size test that was done by DZ. Manuscript draft was done by HG and editing was done by DZ and YP. GM served as the principal investigator of this work and did the final editing.

Competing interests

The corresponding author declares that none of the authors have any competing interest.

Acknowledgement

This work is supported by the Icelandic Research Fund (IRF), grant No. 2008-0445. HG acknowledges the Fulbright Scholar Program, which is sponsored by the U.S. department of state and Fulbright Iceland, that facilitated the stay of HG and her family in Irvine, CA during this work. We also acknowledge high-performance computing support from Cheyenne (doi:10.5065/D6RX99HX) provided by NCAR's Computational and Information Systems Laboratory, sponsored by the National Science Foundation that we used for our experiments. HG wants to thank the staff at the department of Earth System Science at UCI for the facility and assistance during HG's stay at UCI. Finally, we also want to thank Matthew Toohey for his assistance in the interpolation of the forcing files for WACCM4.

 Deleted: Currently, work is ongoing to test the sensitivity of the polar vortex and the emerging SSWs to NH eruptions that are smaller in magnitude as well as the long-term climate impacts. ¶

Deleted:

Deleted: this work

Deleted:

936	References	Deleted: ¶
937	Azoulay, A., Schmidt, H., & Timmreck, C. The Arctic polar vortex response to volcanic forcing of	Deleted: .
938	different strengths. J. Geophys. Res-Atmos., 126(11), e2020JD034450, https://doi.	
939	org/10.1029/2020JD034450 (2021).	
940		
941	Baldwin, M. P., & Dunkerton, T. J. Propagation of the Arctic Oscillation from the stratosphere to	Formatted: Left
942	the troposphere. J. Geophys. Res-Atmos., 104(D24), 30937-30946.	
943	https://doi.org/10.1029/1999JD900445 (1999).	Field Code Changed
944		
945	Barsotti, S., Di Rienzo, D. I., Thordarson, T., Björnsson, B. B., & Karlsdóttir, S. Assessing	Formatted: Left
946	impact to infrastructures due to tephra fallout from Öræfajökull volcano (Iceland) by using a	
947	scenario-based approach and a numerical model. Front. Earth Sci., 6, 196.	
948	https://doi.org/10.3389/feart.2018.00196 (2018).	
949		
950	Bittner M, Schmidt H, Timmreck C, Sienz F. Using a large ensemble of simulations to assess the	
951	Northern Hemisphere stratospheric dynamical response to tropical volcanic eruptions and its	
952	uncertainty. Geophys Res Lett., 43(17), 9324–32, https://doi.org/10.1002/2016GL070587 (2016).	Field Code Changed
953		
954	Bittner, M., Timmreck, C., Schmidt, H., Toohey, M. and Krüger, K. The impact of wave-mean	
955	flow interaction on the Northern Hemisphere polar vortex after tropical volcanic eruptions. J.	
956	Geophys. Res-Atmos., 121(10), 5281-5297, https://doi.org/10.1002/2015JD024603 (2016b).	Field Code Changed
957		
958	Brayshaw, D. J., B. Hoskins, and M. Blackburn. The basic ingredients of the North Atlantic storm	
959	track. Part I: Land-sea contrast and orography. J. Atmos. Sci., 66, 2539–2558,	
960	https://doi.org/10.1175/2009JAS3078.1 (2009).	
961		
962	Brown, F., Marshall, L., Haynes, P. H., Garcia, R. R., Birner, T., & Schmidt, A. On the magnitude	
963	and sensitivity of the quasi-biennial oscillation response to a tropical volcanic eruption. Atmos.	
964	Chem. Phys., 23(9), 5335-5353, https://doi.org/10.5194/acp-23-5335-2023 (2023).	
965		

969	Brugnatelli, V., & Tibaldi, A. Effects in North Africa of the 934-940 CE Eldgjá and 1783-1784	
970	CE Laki eruptions (Iceland) revealed by previously unrecognized written sources. B. Volcanol.,	
971	82(11), 73, https://doi.org/10.1007/s00445-020-01409-0 (2020).	
972		
973	Case, P., Colarco, P. R., Toon, B., Aquila, V., & Keller, C. A. Interactive stratospheric aerosol	Deleted: ¶
974	microphysics-chemistry simulations of the 1991 Pinatubo volcanic aerosols with newly coupled	
975	sectional aerosol and stratosphere-troposphere chemistry modules in the NASA GEOS Chemistry-	
976	Climate Model (CCM). J Adv. Model Earth Sy., 15(8), e2022MS003147.	
977	https://doi.org/10.1029/2022MS003147 (2023).	
978		
979	Charlton-Perez AJ, Ferranti L, Lee RW. The influence of the stratospheric state on North Atlantic	
980	weather regimes. Quart. J. Roy. Meteor. Soc., 144:1140-1151. https://doi.org/10.1002/qj.3280	
981	(2018).	
982		
983	Charlton, A. J., & Polvani, L. M. A_new look at stratospheric sudden warmings. Part I: Climatology	
984	and modeling benchmarks. J. Climate, 20(3), 449-469, https://doi.org/10.1175/JCLI3996.1	
985	(2007).	Deleted:
986		
987	Church, J.A., White, N.J., Arblaster, J.M. Significant decadal-scale impact of volcanic eruptions	
988	on sea level and ocean heat content. Nature 438 (7064), 74–77.	
989	https://doi.org/10.1038/nature04237 (2005).	
990		
991	Chylek, P., Folland, C., Klett, J. D., & Dubey, M. K. CMIP5 climate models overestimate cooling	
992	by volcanic aerosols. Geophys. Res. Lett., 47(3), e2020GL087047.	
993	https://doi.org/10.1029/2020GL087047 (2020).	
994		
995	Clyne, M., Lamarque, JF., Mills, M. J., Khodri, M., Ball, W., Bekki, S., Dhomse, S. S., Lebas,	
996	N., Mann, G., Marshall, L., Niemeier, U., Poulain, V., Robock, A., Rozanov, E., Schmidt, A.,	
997	Stenke, A., Sukhodolov, T., Timmreck, C., Toohey, M., Tummon, F., Zanchettin, D., Zhu, Y., and	
998	Toon, O. B. Model physics and chemistry causing intermodel disagreement within the VolMIP-	Deleted: :

1002	Tambora Interactive Stratospheric Aerosol ensemble, Atmos. Chem. Phys., 21(5), 3317-3343,	Deleted: ,
1003	https://doi.org/10.5194/acp-21-3317-2021, (2021).	Deleted: ,
1004		
1005	Colose CM, LeGrande AN, Vuille M. Hemispherically asymmetric volcanic forcing of tropical	
1006	hydroclimate during the last millennium. Earth Sys Dyn., 7(3), 681-96. doi:10.5194/esd-7-681-	
1007	2016 (2016).	
1008		
1009	DallaSanta, K., Gerber, E. P., & Toohey, M. The circulation response to volcanic eruptions: The	
1010	key roles of stratospheric warming and eddy interactions. J. Clim., 32(4), 1101-1120 (2019).	
1011	DallaSanta, K., & Polvani, L. M. Volcanic stratospheric injections up to 160 Tg (S) yield a Eurasian	Deleted: ←
1012	winter warming indistinguishable from internal variability. Atm. Chem. Phys., 22(13), 8843-8862,	
1013	https://doi.org/10.1175/JCLI-D-18-0099.1 (2022).	Deleted:
1014		
1015	Danabasoglu, G., Lamarque, J.F., Bacmeister, J., Bailey, D.A., DuVivier, A.K., Edwards, J.,	
1016	Emmons, L.K., Fasullo, J., Garcia, R., Gettelman, A. and Hannay, C. The community earth system	Deleted: Danabasoglu, G., Lamarque, J. F., Bacmeister, J.,
1017	model version 2 (CESM2). J Adv. Model Earth Sy., 12(2), e2019MS001916,	Bailey, D. A., DuVivier, A. K., Edwards, J., & Strand, W. G
1018	https://doi.org/10.1029/2019MS001916 (2020).	
1019		
1020	Dee, S. G., Cobb, K. M., Emile-Geay, J., Ault, T. R., Edwards, R. L., Cheng, H., & Charles, C. D.	
1021	No consistent ENSO response to volcanic forcing over the last millennium. Science, 367(6485),	
1022	1477-1481, DOI: 10.1126/science.aax2000 (2020).	
1023		
1024	Ding, X., Chen, G., Zhang, P., Domeisen, D. I., & Orbe, C. Extreme stratospheric wave activity as	
1025	harbingers of cold events over North America. Commun. Earth Environ., 4(1), 187.	
1026	https://doi.org/10.1038/s43247-023-00845-y (2023).	
1027		
1028	Domeisen, D. I., Grams, C. M., & Papritz, L. The role of North Atlantic-European weather regimes	
1029	in the surface impact of sudden stratospheric warming events. Weather Clim. Dynam., 1(2), 373-	
1030	388, https://doi.org/10.5194/wcd-1-373-2020 (2020).	
1 1031		

1039	Driscoll, S., Bozzo, A., Gray, L. J., Robock, A., Stenchikov, G. Coupled Model_Intercomparison		
1040	Project 5 (CMIP5) simulations of climate following volcanic eruptions. J. Geophys. Res-Atmos.		Deleted: -
1041	117 (D17), https://doi.org/10.1029/2012JD017607 (2012).		Field Code Changed
1 1042			
1043	Edmon, H.J., Hoskins, B.J. and McIntyre, M.E. Eliassen-Palm cross sections for the troposphere.		
1044	J. Atmos. Sci., 37, 2600–2616.		
1045	https://doi.org/10.1175/1520-0469(1980)037<2600:EPCSFT>2.0.CO;2 (1980).		Field Code Changed
1 1046			
1047	Einarsson, P. Historical accounts of pre-eruption seismicity of Katla, Hekla, Öræfajökull and other		
1048	volcanoes in Iceland. <i>Jökull</i> , 69, 35-52, https://doi.org/10.33799/jokull2019.69.035 (2019),		Formatted: Font: (Default) Times New Roman
1049			Formatted: Font: (Default) +Body (Aptos)
1050	Elsbury, D., Y. Peings and G. Magnusdottir. Variation in the Holton-Tan effect by longitude. Q. J.		
1051	Roy. Meteor. Soc., DOI: 10.1002/qj.3993 (2021b).		Formatted: Font: Italic
1052			
1053	Elsbury, D., Peings, Y., & Magnusdottir, G. CMIP6 models underestimate the Holton-Tan effect.		
1054	Geophys. Res. Lett., 48(24), e2021GL094083, https://doi.org/10.1029/2021GL094083 (2021).		
1055	Y		Deleted: ¶
1 1056	Fuglestvedt, H. F., Zhuo, Z., Toohey, M., & Krüger, K. Volcanic forcing of high-latitude Northern		Fischer, H., Siggaard-Andersen, M.L., Ruth, U., Röthlisberger, R., Wolff, E. Glacial/interglacial changes in
1057	Hemisphere eruptions. <i>npj Clim. Atmos. Sci.</i> , 7(1), 10, https://doi.org/10.1038/s41612-023-00539-		mineral dust and sea-salt records in polar ice cores: Sources,transport, and deposition. Rev. Geophys. (1), 45
1058	<u>4</u> (2024).		(2007).¶
l 1059			
1060	Gettelman, A., Mills, M.J., Kinnison, D.E., Garcia, R.R., Smith, A.K., Marsh, D.R., Tilmes, S.,		
1061	Vitt, F., Bardeen, C.G., McInerny, J. and Liu, H.L. The whole atmosphere community climate		Deleted: Gettelman, A., Mills, M. J., Kinnison, D. E., Garcia,
1062	model version 6 (WACCM6). J. Geophys. Res-Atmos., 124(23), 12380-12403,		R. R., Smith, A. K., Marsh, D. R., & Randel, W. J
1063	https://doi.org/10.1029/2019JD030943 (2019).		
l 1064			
1065	Gettelman, A., Schmidt, A., & Kristjánsson, J. E. Icelandic volcanic emissions and climate. <i>Nature</i>	**********	Deleted: Egill
1066	Geosci., 8(4), 243-243, https://doi.org/10.1038/ngeo2376 (2015).		
1067			

1078	Gleckler, P.J., AchutaRao, K., Gregory, J.M., Santer, B.D., Taylor, K.E., Wigley, T.M.L. Krakatoa	
1079	lives: The effect of volcanic eruptions on ocean heat content and thermal expansion. Geophys. Res.	Formatted: Font: Italic
1080	Lett. (17), 33, https://doi.org/10.1029/2006GL026771 (2006).	
1081		
1082	Graf, H.F., Perlwitz, J., Kirchner, I. Northern hemisphere tropospheric midlatitude circulation after	
1083	violent volcanic eruptions. Contr. Atmos. Physics 67 (1), 3–13, (1994).	Formatted: Font: Italic
1084	Graf, HF., D. Zanchettin, C. Timmreck and M. Bittner. Observational constraints on the	Deleted: ¶
1085	tropospheric and near-surface winter signature of the Northern Hemisphere stratospheric polar	
1086	vortex. Clim. Dyn., 43, 3245, doi:10.1007/s00382-014-2101-0 (2014).	Formatted: Font: Italic
1087		
1088	Guðlaugsdóttir, H., Steen-Larsen, H. C., Sjolte, J., Masson-Delmotte, V., Werner, M., &	
1089	Sveinbjörnsdóttir, Á. E. The influence of volcanic eruptions on weather regimes over the North	
1090	Atlantic simulated by ECHAM5/MPI-OM ensemble runs from 800 to 2000 CE. Atm. Res., 213,	
1091	211-223, https://doi.org/10.1016/j.atmosres.2018.04.021 (2018).	
1092		
1093	Guðlaugsdóttir, H., Sjolte, J., Sveinbjörnsdóttir, Á. E., Werner, M., & Steen-Larsen, H. C. North	
1094	Atlantic weather regimes in $\delta18O$ of winter precipitation: isotopic fingerprint of the response in	
1095	the atmospheric circulation after volcanic eruptions. Tellus B, 71(1), 1633848.	
1096	https://doi.org/10.1080/16000889.2019.1633848 (2019).	Field Code Changed
1097		
1098	Haynes, P. H. Stratospheric dynamics. Ann. Rev. Fluid Mech., 37(1), 263-293, doi:	
1099	10.1146/annurev.fluid.37.061903.175710 (2005).	
1100		
1101	He, Y., Huang, J. & Ji, M. Impact of land-sea thermal contrast on interdecadal variation in	
1102	circulation and blocking. Clim Dyn. 43, 3267-3279, https://doi.org/10.1007/s00382-014-2103-y	
1103	(2014).	
1104		
1105	Holland, M.M., Hannay, C., Fasullo, J., Jahn, A., Kay, J.E., Mills, M., Simpson, I.R., Wieder, W.,	
1106	Lawrence, P., Kluzek, E. and Bailey, D, New model ensemble reveals how forcing uncertainty and	Deleted: Holland, M. M., Hannay, C., Fasullo, J., Jahn, A.,
1 1107	model structure alter climate simulated across CMIP generations of the Community Earth System	Kay, J. E., Mills, M., & Bailey, D.

1111 Model. Geosci. Model Dev., 17(4), 1585-1602, https://doi.org/10.5194/gmd-17-1585-2024 1112 (2024).1113 1114 Hoskins, B. J., and P. J. Valdes. On the existence of storm-tracks. J. Atmos. Sci., 47, 1854–1864, https://doi.org/10.1175/1520-0469(1990)047<1854:OTEOST>2.0.CO;2 (1990). 1115 1116 1117 Huang, J., Hitchcock, P., Maycock, A. C., McKenna, C. M., & Tian, W. Northern hemisphere cold 1118 air outbreaks are more likely to be severe during weak polar vortex conditions. Commun. Earth 1119 Environ., 2(1), 147, https://doi.org/10.1038/s43247-021-00215-6 (2021). 1120 1121 Hurrell, J.W. Decadal trends in the north atlantic oscillation: regional tempera-tures and 1122 precipitation. Science 269 (5224), 676-679, DOI: 10.1126/science.269.5224.676 (1995). Formatted: Font: Italic 1123 1124 Hurrell, J.W., Holland, M.M., Gent, P.R., Ghan, S., Kay, J.E., Kushner, P.J., Lamarque, J.F., Large, 1125 W.G., Lawrence, D., Lindsay, K. and Lipscomb., The community earth system model: a framework Deleted: Hurrell, J. W., Holland, M. M., Gent, P. R., Ghan, S., Kay, J. E., Kushner, P. J., ... & Marshall, S. 1126 collaborative research. В. Meteorol. 94(9), 1339-1360, Am. Soc., 1127 https://doi.org/10.1175/BAMS-D-12-00121.1 (2013). 1128 1129 Ineson, S., Dunstone, N. J., Scaife, A. A., Andrews, M. B., Lockwood, J. F., & Pang, B. Statistics 1130 of sudden stratospheric warmings using a large model ensemble. Atmos. Sci. Lett., 25(3), e1202, 1131 https://doi.org/10.1002/asl.1202 (2023). Deleted: 4 1132 Jungclaus, J. H., Bard, E., Baroni, M., Braconnot, P., Cao, J., Chini, L. P., Egorova, T., Evans, M., 1133 1134 González-Rouco, J. F., Goosse, H., Hurtt, G. C., Joos, F., Kaplan, J. O., Khodri, M., Klein Goldewijk, K., Krivova, N., LeGrande, A. N., Lorenz, S. J., Luterbacher, J., Man, W., Maycock, 1135 1136 A. C., Meinshausen, M., Moberg, A., Muscheler, R., Nehrbass-Ahles, C., Otto-Bliesner, B. I., Phipps, S. J., Pongratz, J., Rozanov, E., Schmidt, G. A., Schmidt, H., Schmutz, W., Schurer, A., 1137 Shapiro, A. I., Sigl, M., Smerdon, J. E., Solanki, S. K., Timmreck, C., Toohey, M., Usoskin, I. G., 1138 1139 Wagner, S., Wu, C.-J., Yeo, K. L., Zanchettin, D., Zhang, Q., and Zorita, E.: The PMIP4 contribution to CMIP6 - Part 3: The last millennium, scientific objective, and experimental design 1140

1144	for the PMIP4 past1000 simulations, Geosci. Model Dev., 10, 4005-4033,		Deleted: ,
1145	https://doi.org/10.5194/gmd-10-4005-2017, (2017).	****	Formatted: Font: Italic
1146			
1147	Karami, K., Braesicke, P., Sinnhuber, M., and Versick, S. On the climatological probability of the		
1148	vertical propagation of stationary planetary waves. Atmos. Chem. Phys., 16, 8447-8460,		Deleted: ,
1149	https://doi.org/10.5194/acp-16-8447-2016 (2016).		Formatted: Font: Italic
1150			
1151	Khodri, M., Izumo, T., Vialard, J., Janicot, S., Cassou, C., Lengaigne, M., Mignot, J., Gastineau,		
1152	G., Guilyardi, E., Lebas, N. and Robock, A. Tropical explosive volcanic eruptions can trigger El		Deleted: Khodri, M., Izumo, T., Vialard, J., Janicot, S.,
1153	Niño by cooling tropical Africa. Nat. Commun., 8(1), 778. https://doi.org/10.1038/s41467-017-		Cassou, C., Lengaigne, M., et al Formatted: Font: Italic
1154	<u>00755-6 (</u> 2017).	,	
1155			
1156	Kim, B.M., Son, S.W., Min, S.K., Jeong, J.H., Kim, S.J., Zhang, X., Shim, T., Yoon, J.H.		
1157	Weakening of the stratospheric polar vortex by arctic sea-ice loss. Nat. Commun., 5, 4646,		Formatted: Font: Italic
1158	https://doi.org/10.1038/ncomms5646 (2014).		
1159			
1160	Kodera, K. Influence of volcanic eruptions on the troposphere through strato-spheric dynamical		
1161	processes in the northern hemisphere winter. J. Geophys. ResAtmos., 99 (D1), 1273–1282,		Formatted: Font: Italic
1162	https://doi.org/10.1029/93JD02731 (1994).		
1 1163			
1164	Kodera, K., Mukougawa, H., Maury, P., Ueda, M., & Claud, C. Absorbing and reflecting sudden		
1165	stratospheric warming events and their relationship with tropospheric circulation. J. Geophys. Res-		
1166	Atmos., 121(1), 80-94, https://doi.org/10.1002/2015JD023359 (2016).		Field Code Changed
1 1167			
1168	Kolstad, E. W., Lee, S. H., Butler, A. H., Domeisen, D. I., & Wulff, C. O. Diverse surface signatures		
1169	of stratospheric polar vortex anomalies. J. Geophys. Res-Atmos., 127(20), e2022JD037422,		
1170	https://doi.org/10.1029/2022JD037422 (2022).		
1171			
1172	Kretschmer, M., Cohen, J., Matthias, V., Runge, J., & Coumou, D. The different stratospheric		
1173	influence on cold-extremes in Eurasia and North America. npj Clim. Atmos. Sci., 1(1), 44,		
1174	https://doi.org/10.1038/s41612-018-0054-4 (2018).		
•			

1179		
1180	Labe, Z., Peings, Y., & Magnusdottir, G. The effect of QBO phase on the atmospheric response to	
1181	projected Arctic sea ice loss in early winter. Geophys. Res. Lett., 46(13), 7663-7671,	
1182	https://doi.org/10.1029/2019GL083095_(2019).	Deleted:
ا 1183		Formatted: Font: (Default) Times New Roman
1184	Larsen, G., & Gudmundsson, M. T. Volcanic system: Bárðarbunga system. Catalogue of Icelandic	
1185	Volcanoes, 1-11 (2014).	
1186	Lehtonen, I., & Karpechko, A. Y. Observed and modeled tropospheric cold anomalies associated	Deleted: ¶
1187	with sudden stratospheric warmings. J. Geophys. Res-Atmos., 121(4), 1591-1610,	
1188	https://doi.org/10.1002/2015JD023860 (2016).	
1 1189		
1190	Ma, J., Chen, W., Yang, R. et al. Downward propagation of the weak stratospheric polar vortex	
1191	events: the role of the surface arctic oscillation and the quasi-biennial oscillation. <i>Clim. Dyn.</i> , 62,	Formatted: Font: Italic
1 1192	4117–4131 https://doi.org/10.1007/s00382-024-07121-5 (2024).	
1193		
1194	Matsuno, T. Vertical propagation of stationary planetary waves in the winter Northern Hemisphere.	Deleted: ,
1195	J. Atmos. Sci., 27, 871–883. 32291, 32292, 32294, 32296, 32306, https://doi.org/10.1175/1520-	Formatted: Font: Italic
1196	0469(1970)027<0871:VPOSPW>2.0.CO;2 (1970).	
1 1197		
1198	Meronen, H., Henriksson, S. V., Räisänen, P., & Laaksonen, A. Climate effects of northern	
1199	hemisphere volcanic eruptions in an Earth System Model. Atmos. Res., 114, 107-118,	
1200	https://doi.org/10.1016/j.atmosres.2012.05.011 (2012).	
1201	V.	Deleted: ¶
1202	Muthers, S., Raible, C. C., Rozanov, E., & Stocker, T. F. Response of the AMOC to reduced solar	
1203	radiation-the modulating role of atmospheric chemistry. Earth Syst. Dynam., 7(4), 877-892,	
1204	https://doi.org/10.5194/esd-7-877-2016 (2016).	
1205		
1206	Nakamura, N. Large-Scale Eddy-Mean Flow Interaction in the Earth's Extratropical	
1207	Atmosphere. Annu. Rev. Fluid Mech., 56(1), 349-377, https://doi.org/10.1146/annurev-fluid-	
1208	<u>121021-035602</u> (2024).	
1209		

4045	16 1 4 1 4 1 4 1 4 1 4 C 4 1 7 4 1 9 4 M 11 (GE9M) C		
1215	aerosol for both radiation and chemistry in the Community Earth System Model (CESM1). <i>Geosci</i> .		
1216	Model Dev., 9(7), 2459-2470, https://doi.org/10.5194/gmd-9-2459-2016 (2016).		
1217			
1218	Oman, L., Robock, A., Stenchikov, G., Schmidt, G. A., & Ruedy, R. Climatic response to high-		
1219	latitude volcanic eruptions. J. Geophys. Res-Atmos., 110(D13).		
1220	https://doi.org/10.1029/2004JD005487 (2005).		
1221	Omrani, NE., Keenlyside, N., Matthes, K., Boljka, L., Zanchettin, D., Jungclaus, J. H., Lubis, S.		Deleted: ¶
1222	W. Coupled stratosphere-troposphere-Atlantic multidecadal oscillation and its importance for		
1223	near-future climate projection. npj Clim. Atmos. Sci, 5, 59, https://doi.org/10.1038/s41612-022-		
1224	<u>00275-1 (2022).</u>		
1225			
1226	Oppenheimer, C., Orchard, A., Stoffel, M., Newfield, T.P., Guillet, S., Corona, C., Sigl, M., Di		
1227	Cosmo, N. and Büntgen, U, The Eldgjá eruption: timing, long-range impacts and influence on the		Deleted: Oppenheimer, C., Orchard, A., Stoffel, M.,
1228	Christianisation of Iceland. Climatic Change, 147, 369-381, https://doi.org/10.1007/s10584-018-	l	Newfield, T. P., Guillet, S., Corona, C., & Büntgen, U.
1229	<u>2171-9 (2018)</u> .		
1230			
1231	Otterå, O.H., Bentsen, M., Drange, H., Suo, L., 2010. External forcing as a metronome foratlantic		
1232	multidecadal variability. Nat. Geosci., 3 (10), 688–694, https://doi.org/10.1038/ngeo955 (2018).		Formatted: Font: Italic
l 1233			
1234	Ortega, P., Swingedouw, D., Masson-Delmotte, V., Risi, C., Vinther, B., Yiou, P., Vautard, R.,		
1235	Yoshimura, K. Characterizing atmospheric circulation signals in. Greenlandice cores: insights		
1236	from a weather regime approach. Clim. Dyn., 43 (9–10), 2585–2605, doi: 10.1007/S00382-014-		Formatted: Font: Italic
1237	2074-Z (2014).		Formatted: Font: Not Bold
1238			Deleted: ¶
Т 1239	Pausata, F. S. R., Chafik, L., Caballero, R. & Battisti, D. S. Impacts of high-latitude volcanic		Otterå, O. H., Bentsen, M., Drange, H., & Suo, L. External forcing as a metronome for Atlantic multidecadal
1240	eruptions on ENSO and AMOC. Proc. Natl Acad. Sci., 112, 13784–13788,		variability. Nat. Geosci, 3(10), 688-694 (2010).
1241	https://doi.org/10.1073/pnas.1509153112 (2015).		Formatted: Font: Italic
	<u>πτρο.// του.ουχ/10.1075/μπαδ.1507155112</u> (2015).		
1242			

Neely III, R. R., Conley, A. J., Vitt, F., & Lamarque, J. F. A consistent prescription of stratospheric

extratropical teleconnections drive ENSO response to volcanic eruptions. Sci. Adv., 6(23) Formatted: Font	Italic
1050 5000 1: 10.1100/ : 1 5000 (2020)	
1252 eaaz5006, doi: 10.1126/sciadv.aaz5006 (2020).	
1253	
Pausata, F. S. R., Zhao, Y., Zanchettin, D., Caballero, R., & Battisti, D. S. Revisiting the	
mechanisms of ENSO response to tropical volcanic eruptions. <i>Geophys. Res. Lett.</i> , 50, Formatted: Font	Italic
1256 e2022GL102183. https://doi.org/10.1029/2022GL102183 (2023).	
1257	
1258 Perlwitz, J., Graf, H.F. The statistical connection between tropospheric and. stra-tospheric	
1259 circulation of the Northern Hemisphere in winter. J. Clim., (10),2281–2295, Formatted: Font	Italic
1260 <u>https://doi.org/10.1175/1520-0442(1995)008<2281:TSCBTA>2.0.CO;2</u> (1995).	
1261	
Peings, Y., & Magnusdottir, G. Response of the wintertime Northern Hemisphere atmospheric	
1263 circulation to current and projected Arctic sea ice decline: A numerical study with CAM5. J. Clim.,	
1264 27(1), 244-264 <u>, https://doi.org/10.1175/JCLI-D-13-00272.1</u> (2014).	
1265	
1266 Peings, Y., Davini, P., & Magnusdottir, G. Impact of Ural blocking on early winter climate	
1267 variability under different Barents-Kara sea ice conditions. J. Geophys. Res-Atmos., 128(6),	
1268 e2022JD036994 <u>, https://doi.org/10.1029/2022JD036994</u> (2023).	
1 1269	
Plumb, R. A. On the three-dimensional propagation of stationary waves. J. Atmos. Sci., 42(3), 217-	
1271 229, https://doi.org/10.1175/1520-0469(1985)042<0217:OTTDPO>2.0.CO;2 (1985).	
1272	
Polvani, L. M., Banerjee, A., & Schmidt, A. Northern Hemisphere continental winter warming	
following the 1991 Mt. Pinatubo eruption: reconciling models and observations. <i>Atmos. Chem.</i>	
1275 Phys., 19(9), 6351-6366, https://doi.org/10.5194/acp-19-6351-2019 (2019).	
1276	
1277 Portal, A., Pasquero, C., D'andrea, F., Davini, P., Hamouda, M. E., & Rivière, G. Influence of Deleted:	
reduced winter land–sea contrast on the midlatitude atmospheric circulation. J. Clim., 35(19),	
1279 6237-6251, https://doi.org/10.1175/JCLI-D-21-0941.1 (2022).	
1 1280	

1282	Predybaylo, E., Stenchikov, G., Wittenberg, A. T. & Osipov, S. El Niño/ Southern Oscillation		
1283	response to low-latitude volcanic eruptions depends on ocean pre-conditions and eruption timing.		
1284	Commun. Earth Environ., 1, 1–13, https://doi.org/10.1038/s43247-020-0013-y (2020).		Formatted: Font: Italic
1285			
1286	Rayner, N.A.A., Parker, D.E., Horton, E.B., Folland, C.K., Alexander, L.V., Rowell, D.P., Kent,		
1287	E.C. and Kaplan, A. Global analyses of sea surface temperature, sea ice, and night marine air		Deleted: Rayner, N. A. A., Parker, D. E., Horton, E. B., Folland, C. K., Alexander, L. V., Rowell, D. P., & Kaplan,
1288	temperature since the late nineteenth century. J. Geophys. Res-Atmos., 108(D14).		A A Rexander, L. v., Rowell, D. P., & Rapian,
1289	https://doi.org/10.1029/2002JD002670 (2003).		
1290	Robock, A., Mao, J. Winter warming from large volcanic eruptions. <i>Geophys. Res.Lett.</i> , 19 (24),	~	Deleted: ¶
1291	2405–2408, https://doi.org/10.1029/92GL02627 (1992).		Formatted: Font: Italic
1292			
1293	Robock, A. Volcanic eruptions and climate. Rev. Geophys., 38 (2), 191-219,		Formatted: Font: Italic
1294	https://doi.org/10.1029/1998RG000054 (2000).		
1295			
1296	Screen, J.A., Deser, C., Smith, D.M., Zhang, X., Blackport, R., Kushner, P.J., Oudar, T., McCusker,		
1297	K.E. and Sun, L, Consistency and discrepancy in the atmospheric response to Arctic sea-ice loss		Deleted: Screen, J. A., Deser, C., Smith, D. M., Zhang, X.,
1298	across climate models. Nat. Geosci., 11(3), 155-163, https://doi.org/10.1038/s41561-018-0059-y	(Blackport, R., Kushner, P. J., & Sun, L. Deleted:
1299	(2018).		
1300			
1301	Shindell, D.T., Schmidt, G.A., Mann, M.E., Faluvegi, G. Dynamic winter. Climate response to		
1802	large tropical volcanic eruptions since 1600. J. Geophys. ResAtmos,. (D5), 109,		Formatted: Font: Italic
1803	https://doi.org/10.1029/2003JD004151 (2004).		
1304			
1305	Sigl, M., Winstrup, M., McConnell, J.R., Welten, K.C., Plunkett, G., Ludlow, F., Buntgen, U.,		
1306	Caffee, M., Chellman, N., Dahl-Jensen, D., Fischer, H., 2009. Timing and climate forcing of		
1807	volcanic eruptions for the past 2500 years. Nature 523 (7562), 543-549,		Formatted: Font: Italic
1308	https://doi.org/10.1038/nature14565 (2015).		Deleted: 09
1309			
1310	Sjolte, J., Adolphi, F., Guðlaugsdóttir, H., & Muscheler, R. Major Differences in Regional Climate		
1311	Impact Between High-and Low-Latitude Volcanic Eruptions. Geophys. Res. Lett., 48(8),		
1812	e2020GL092017 <u>, https://doi.org/10.1029/2020GL092017</u> (2021).		Field Code Changed

1322	Smith, D.M., Eade, R., Andrews, M.B., Ayres, H., Clark, A., Chripko, S., Deser, C., Dunstone,	Deleted: ¶
1323	N.J., García-Serrano, J., Gastineau, G. and Graff, L.S., Robust but weak winter atmospheric	Deleted: Smith, D. M., Eade, R., Andrews, M. B., Ayres, H.,
1324	circulation response to future Arctic sea ice loss. Nat. Commun., 13(1), 727,	Clark, A., Chripko, S., & Walsh, A.
1325	https://doi.org/10.1038/s41467-022-28283-y (2022)	Deleted: .
1326		
1327	Smith, K. L., Neely, R. R., Marsh, D. R., & Polvani, L. M. The specified chemistry whole	
1828	atmosphere community climate model (SC-WACCM). J. Adv. Model Earth Sy., 6(3), 883-901.	
1329	https://doi.org/10.1002/2014MS000346 (2014).	
1330		
1331	Stenchikov, G., Robock, A., Ramaswamy, V., Schwarzkopf, M.D., Hamilton, K., Ramachandran,	
1332	S. Arctic Oscillation response to the 1991 Mount Pinatubo.eruption: Effects of volcanic aerosols	
1333	and ozone depletion. J. Geophys. ResAtmos., (D24), 107,	Deleted: .
1334	https://doi.org/10.1029/2002JD002090 (2002).	Formatted: Font: Italic
1335		
1336	Stenchikov, G., Delworth, T.L., Ramaswamy, V., Stouffer, R.J., Wittenberg, A., Zeng, F. Volcanic	
1337	signals in oceans. J. Geophys. ResAtmos., (D16), 114, https://doi.org/10.1029/2008JD011673	Deleted: .
1338	(2009).	Formatted: Font: Italic
1339		Field Code Changed
1340	Stothers, R. B. Far reach of the tenth century Eldgjá eruption, Iceland. Climatic Change, 39(4),	
1341	715-726, https://doi.org/10.1023/A:1005323724072 (1998).	
1 1342		
1343	Swingedouw, D., Ortega, P., Mignot, J., Guilyardi, E., Masson-Delmotte, V., Butler, P.G., Khodri,	
1344	M., Séférian, R. Bidecadal North Atlantic ocean circulation variability controlled by timing of	
1345	volcanic eruptions. Nat. Commun., 6, 6545, https://doi.org/10.1038/ncomms7545 (2015).	
1346		
1347	Thomas, M. A., Giorgetta, M. A., Timmreck, C., Graf, H. F., & Stenchikov, G. Simulation of the	
1348	climate impact of Mt. Pinatubo eruption using ECHAM5-Part 2: Sensitivity to the phase of the	
1849	QBO and ENSO. Atmos. Chem. Phys., 9(9), 3001-3009, https://doi.org/10.5194/acp-9-3001-2009	
1350	(2009).	
1351		
	40	

1358	Timmreck, C.: Modeling the climatic effects of large explosive volcanic eruptions, Wiley	Deleted: ,
1359	Interdisciplinary Reviews: Climate Change, 3, 545–564, https://doi.org/10.1002/wcc.192 (2012).	Formatted: Font: Italic
1360		
1361	Thordarson, T., & Self, S. Atmospheric and environmental effects of the 1783–1784 Laki eruption:	
1362	A review and reassessment. J. Geophys. ResAtmos., 108(D1), AAC-7.	
1363	https://doi.org/10.1029/2001JD002042 (2003).	
1364	Thordarson, T., Miller, D. J., Larsen, G., Self, S., & Sigurdsson, H. New estimates of sulfur	Deleted: ¶
1365	degassing and atmospheric mass-loading by the 934 AD Eldgjá eruption, Iceland. J. Volcanol.	
1366	Geoth. Res., 108(1-4), 33-54, https://doi.org/10.1016/S0377-0273(00)00277-8 (2001).	
1367		
1368	Toohey, M., Stevens, B., Schmidt, H., & Timmreck, C. Easy Volcanic Aerosol (EVA v1. 0): an	
1369	idealized forcing generator for climate simulations. Geosci. Model Dev., 9(11), 4049-4070,	
1370	https://doi.org/10.5194/gmd-9-4049-2016 (2016).	
1371		
1372	Toohey, M., Krüger, K., Schmidt, H., Timmreck, C., Sigl, M., Stoffel, M., & Wilson, R.	
1873	Disproportionately strong climate forcing from extratropical explosive volcanic eruptions. Nat.	Formatted: Font: Italic
1873 1874	Disproportionately strong climate forcing from extratropical explosive volcanic eruptions. <i>Nat. Geosci.</i> 12(2), 100-107, https://doi.org/10.1038/s41561-018-0286-2 (2019).	Formatted: Font: Italic Formatted: Font: Italic
1374		
1874 1375	Geosci, 12(2), 100-107, https://doi.org/10.1038/s41561-018-0286-2 (2019).	
1874 1375 1376	Geosci, 12(2), 100-107, https://doi.org/10.1038/s41561-018-0286-2 (2019). Toohey, M., Krüger, K., Bittner, M., Timmreck, C., and Schmidt, H.: The impact of volcanic	
1374 1375 1376 1377	Geosci, 12(2), 100-107, https://doi.org/10.1038/s41561-018-0286-2 (2019). Toohey, M., Krüger, K., Bittner, M., Timmreck, C., and Schmidt, H.: The impact of volcanic aerosol on the Northern Hemisphere stratospheric polar vortex: mechanisms and sensitivity to	Formatted: Font: Italic
1374 1375 1376 1377 1378	Geosci, 12(2), 100-107, https://doi.org/10.1038/s41561-018-0286-2 (2019). Toohey, M., Krüger, K., Bittner, M., Timmreck, C., and Schmidt, H.: The impact of volcanic aerosol on the Northern Hemisphere stratospheric polar vortex: mechanisms and sensitivity to forcing structure, Atmos. Chem. Phys., 14, 13063–13079, https://doi.org/10.5194/acp-14-13063-	Formatted: Font: Italic Formatted: Font: Italic
1874 1375 1376 1377 1878 1879	Geosci, 12(2), 100-107, https://doi.org/10.1038/s41561-018-0286-2 (2019). Toohey, M., Krüger, K., Bittner, M., Timmreck, C., and Schmidt, H.: The impact of volcanic aerosol on the Northern Hemisphere stratospheric polar vortex: mechanisms and sensitivity to forcing structure, Atmos. Chem. Phys., 14, 13063–13079, https://doi.org/10.5194/acp-14-13063-	Formatted: Font: Italic Formatted: Font: Italic
1374 1375 1376 1377 1378 1379	Geosci, 12(2), 100-107, https://doi.org/10.1038/s41561-018-0286-2 (2019). Toohey, M., Krüger, K., Bittner, M., Timmreck, C., and Schmidt, H.: The impact of volcanic aerosol on the Northern Hemisphere stratospheric polar vortex: mechanisms and sensitivity to forcing structure, Atmos. Chem. Phys., 14, 13063–13079, https://doi.org/10.5194/acp-14-13063-2014, (2014).	Formatted: Font: Italic Formatted: Font: Italic
1374 1375 1376 1377 1378 1379 1380 1381	Geosci, 12(2), 100-107, https://doi.org/10.1038/s41561-018-0286-2 (2019). Toohey, M., Krüger, K., Bittner, M., Timmreck, C., and Schmidt, H.: The impact of volcanic aerosol on the Northern Hemisphere stratospheric polar vortex: mechanisms and sensitivity to forcing structure, Atmos. Chem. Phys., 14, 13063–13079, https://doi.org/10.5194/acp-14-13063-2014 (2014). Wake, B. Land–sea contrast. Nat. Clim. Change 4., 326, https://doi.org/10.1038/nclimate2233	Formatted: Font: Italic Formatted: Font: Italic
1374 1375 1376 1377 1378 1379 1380 1381	Geosci, 12(2), 100-107, https://doi.org/10.1038/s41561-018-0286-2 (2019). Toohey, M., Krüger, K., Bittner, M., Timmreck, C., and Schmidt, H.: The impact of volcanic aerosol on the Northern Hemisphere stratospheric polar vortex: mechanisms and sensitivity to forcing structure, Atmos. Chem. Phys., 14, 13063–13079, https://doi.org/10.5194/acp-14-13063-2014 (2014). Wake, B. Land–sea contrast. Nat. Clim. Change 4., 326, https://doi.org/10.1038/nclimate2233	Formatted: Font: Italic Formatted: Font: Italic
1374 1375 1376 1377 1378 1379 1380 1381 1382 1383	Geosci, 12(2), 100-107, https://doi.org/10.1038/s41561-018-0286-2 (2019). Toohey, M., Krüger, K., Bittner, M., Timmreck, C., and Schmidt, H.: The impact of volcanic aerosol on the Northern Hemisphere stratospheric polar vortex: mechanisms and sensitivity to forcing structure, Atmos. Chem. Phys., 14, 13063–13079, https://doi.org/10.5194/acp-14-13063-2014 (2014). Wake, B. Land–sea contrast. Nat. Clim. Change 4., 326, https://doi.org/10.1038/nclimate2233 (2014).	Formatted: Font: Italic Formatted: Font: Italic
1374 1375 1376 1377 1378 1379 1380 1381 1382 1383	Geosci, 12(2), 100-107, https://doi.org/10.1038/s41561-018-0286-2 (2019). Toohey, M., Krüger, K., Bittner, M., Timmreck, C., and Schmidt, H.: The impact of volcanic aerosol on the Northern Hemisphere stratospheric polar vortex: mechanisms and sensitivity to forcing structure, Atmos. Chem. Phys., 14, 13063–13079, https://doi.org/10.5194/acp-14-13063-2014, (2014). Wake, B. Land–sea contrast. Nat. Clim. Change 4., 326, https://doi.org/10.1038/nclimate2233 (2014). Weierbach, H., LeGrande, A. N., and Tsigaridis, K.: The impact of ENSO and NAO initial	Formatted: Font: Italic Formatted: Font: Italic Deleted: ,

1392	Yu, Q., Wu, B., & Zhang, W. The atmospheric connection between the Arctic and Eurasia is		
1393	underestimated in simulations with prescribed sea ice. Commun. Earth Environ., 5(1), 435,		Formatted: Font: Italic
1394	https://doi.org/10.1038/s43247-024-01605-2 (2024).		
1395			
1396	Zambri, B., Robock, A., Mills, M. J., & Schmidt, A. Modeling the 1783-1784 Laki eruption in		
1397	Iceland: 2. Climate impacts. J. Geophys. ResAtmos., 124(13), 6770-6790.		
1398	https://doi.org/10.1029/2018JD029554 (2019).		
1399	Zambri B, Slawinska J, Robock A, LeGrande AN. Northern Hemisphere Winter Warming and		Deleted: ¶
1400	Summer Monsoon Reduction after Volcanic Eruptions over the Last Millennium. J. Geophys., Res.,	;;;(Formatted: Font: Italic
1401	Atmos., 122 (15):7971-7989. doi: 10.1002/2017jd026728 (2017).		Formatted: Font: Italic
1 1402		1	Formatted: Font: Italic Formatted: Font: Italic
1403	Zanchettin, D., Timmreck, C., Graf, H.F., Rubino, A., Lorenz, S., Lohmann, K., Jungclaus, J.H. Bi-	(romatted. Folit. Italic
1404	decadal variability excited in the coupled ocean-atmosphere system by strong tropical volcanic		
1405	eruptions. <i>Clim. Dyn.</i> , 39 (1–2), 419–444, https://doi.org/10.1007/s00382-011-1167-1 (2012).		Formatted: Font: Italic
l 1406			
1407	Zanchettin, D., Timmreck, C., Bothe, O., Lorenz, S.J., Hegerl, G., Graf, H.F., Lutherbacher, J.,		
1408	Jungclaus, J.H. Delayed winter warming: A robust decadal response to strong tropical volcanic		
1409	eruptions. <i>Geophys. Res. Lett.</i> , 40 (1), 204–209, https://doi.org/10.1029/2012GL054403 (2013).		Formatted: Font: Italic
1410			Field Code Changed
1411	Zanchettin, D., Khodri, M., Timmreck, C., Toohey, M., Schmidt, A., Gerber, E. P., Hegerl, G.,		
1412	Robock, A., Pausata, F. S. R., Ball, W. T., Bauer, S. E., Bekki, S., Dhomse, S. S., LeGrande, A. N.,		
1413	Mann, G. W., Marshall, L., Mills, M., Marchand, M., Niemeier, U., Poulain, V., Rozanov, E.,		
1414	Rubino, A., Stenke, A., Tsigaridis, K., and Tummon, F.: The Model Intercomparison Project on the		
1415	climatic response to Volcanic forcing (VolMIP): experimental design and forcing input data for		
1416	CMIP6 Geosci. Model Dev., 9, 2701-2719, doi:10.5194/gmd-9-2701-2016 (2016).	e:(Deleted: ,
1417			Deleted: ,
1418	Zanchettin, D., C. Timmreck, M. Toohey, J. H. Jungclaus, M. Bittner, S. J. Lorenz, A. Rubino.	7	Formatted: Font: Italic
1419	Clarifying the Relative Role of Forcing Uncertainties and Initial-Condition Unknowns in		
1420	Spreading the Climate Response to Volcanic Eruptions. Geophys. Res. Lett., 46, 1602-1611,		Formatted: Font: Italic
1421	https://doi.org/10.1029/2018GL081018 (2019).		

1426	Zanchettin, D. Aerosol and Solar Irradiance Effects on Decadal Climate Variability and		
1427	Predictability. Current Climate Change Reports, 3, 150, doi:10.1007/s40641-017-0065-y (2017).		
1 1428			
1429	Zanchettin, D., Timmreck, C., Khodri, M., Schmidt, A., Toohey, M., Abe, M., Bekki, S., Cole, J.,		
1430	Fang, SW., Feng, W., Hegerl, G., Johnson, B., Lebas, N., LeGrande, A. N., Mann, G. W.,		
1431	Marshall, L., Rieger, L., Robock, A., Rubinetti, S., Tsigaridis, K., and Weierbach, H, Effects of		Deleted: :
1432	forcing differences and initial conditions on inter-model agreement in the VolMIP volc-pinatubo-		
1433	full experiment_Geosci. Model Dev., 15, 2265-2292, https://doi.org/10.5194/gmd-15-2265-2022		Deleted: ,
1434	(2022).	1	Deleted: ,
1435			Formatted: Font: Italic
1436	Zhang, P., Wu, Y., Simpson, I. R., Smith, K. L., Zhang, X., De, B., & Callaghan, P. A stratospheric		
1437	pathway linking a colder Siberia to Barents-Kara Sea sea ice loss. Sci. Adv., 4(7), eaat6025,		
1438	DOI: 10.1126/sciadv.aat6025 (2018).		
1439			
1440	Zhang, R., Tian, W., Zhang, J., Huang, J., Xie, F., & Xu, M. The corresponding tropospheric		
1441	environments during downward-extending and nondownward-extending events of stratospheric		
1442	northern annular mode anomalies. J. Clim., 32(6), 1857-1873, https://doi.org/10.1175/JCLI-D-18-		
1443	<u>0574.1</u> (2019).		
1444			
1445	Zhu, F., Emile-Geay, J., Anchukaitis, K.J., Hakim, G.J., Wittenberg, A.T., Morales, M.S., Toohey,		
1446	M. and King, J, A re-appraisal of the ENSO response to volcanism with paleoclimate data		Deleted: Zhu, F., Emile-Geay, J., Anchukaitis, K. J., Hakim,
1447	assimilation. Nat. Commun., 13(1), 747, https://doi.org/10.1038/s41467-022-28210-1 (2022).		G. J., Wittenberg, A. T., Morales, M. S., & King, J.
1448			
1449	Zhuo, Z., Fuglestvedt, H. F., Toohey, M., and Krüger, K, Initial atmospheric conditions control		Deleted: :
1450	transport of volcanic volatiles, forcing and impacts, Atmos. Chem. Phys., 24, 6233-6249,		Deleted: ,
1451	https://doi.org/10.5194/acp-24-6233-2024, (2024).		Formatted: Font: Italic
1 1452			Deleted: ,
1453			
1454			